SANDIA REPORT

SAND2010-3284
Unlimited Release
Printed April, 2011

Analytic 1D *pn* junction diode photocurrent solutions following ionizing radiation and including time-dependent changes in the carrier lifetime

Bert Kerr, Carl L. Axness, and Eric R. Keiter

Prepared by
Sandia National Laboratories
Albuquerque, New Mexico 87185 and Livermore, California 94550

Sandia National Laboratories is a multi-program laboratory managed and operated by Sandia Corporation, a wholly owned subsidiary of Lockheed Martin Corporation, for the U.S. Department of Energy's National Nuclear Security Administration under contract DE-AC04-94AL85000.

Approved for public release; further dissemination unlimited.

Sandia National Laboratories

Issued by Sandia National Laboratories, operated for the United States Department of Energy by Sandia Corporation.

NOTICE: This report was prepared as an account of work sponsored by an agency of the United States Government. Neither the United States Government, nor any agency thereof, nor any of their employees, nor any of their contractors, subcontractors, or their employees, make any warranty, express or implied, or assume any legal liability or responsibility for the accuracy, completeness, or usefulness of any information, apparatus, product, or process disclosed, or represent that its use would not infringe privately owned rights. Reference herein to any specific commercial product, process, or service by trade name, trademark, manufacturer, or otherwise, does not necessarily constitute or imply its endorsement, recommendation, or favoring by the United States Government, any agency thereof, or any of their contractors or subcontractors. The views and opinions expressed herein do not necessarily state or reflect those of the United States Government, any agency thereof, or any of their contractors.

Printed in the United States of America. This report has been reproduced directly from the best available copy.

Available to DOE and DOE contractors from
U.S. Department of Energy
Office of Scientific and Technical Information
P.O. Box 62
Oak Ridge, TN 37831

Telephone: (865) 576-8401
Facsimile: (865) 576-5728
E-Mail: reports@adonis.osti.gov
Online ordering: http://www.osti.gov/bridge

Available to the public from
U.S. Department of Commerce
National Technical Information Service
5285 Port Royal Rd
Springfield, VA 22161

Telephone: (800) 553-6847
Facsimile: (703) 605-6900
E-Mail: orders@ntis.fedworld.gov
Online ordering: http://www.ntis.gov/help/ordermethods.asp?loc=7-4-0#online

SAND2010-3284
Unlimited Release
Printed April, 2011

Analytic 1D *pn* junction diode photocurrent solutions following ionizing radiation and including time-dependent changes in the carrier lifetime

Bert Kerr, Carl L. Axness, and Eric R. Keiter

Abstract

Circuit simulation tools (e.g., **SPICE** [1]) have become invaluable in the development and design of electronic circuits in radiation environments. These codes are often employed to study the effect of many thousands of devices under transient current conditions. Device-scale simulation tools (e.g., **MEDICI** [2]) are commonly used in the design of individual semiconductor components, but require computing resources that make their incorporation into a circuit code impossible for large-scale circuits. Analytic solutions to the ambipolar diffusion equation, an approximation to the carrier transport equations, may be used to characterize the transient currents at nodes within a circuit simulator. We present new transient 1D excess carrier density and photocurrent density solutions to the ambipolar diffusion equation for low-level radiation pulses that take into account a finite device geometry, ohmic fields outside the depleted region, and an arbitrary change in the carrier lifetime due to neutron irradiation or other effects. The solutions are specifically evaluated for the case of an abrupt change in the carrier lifetime during or after, a step, square, or piecewise linear radiation pulse. Noting slow convergence of the raw Fourier series for certain parameter sets, we use closed-form formulas for some of the infinite sums to produce "partial closed-form" solutions for the above three cases. These "partial closed-form" solutions converge with only a few tens of terms, which enables efficient large-scale circuit simulations.

Contents

1 Introduction 9
2 Mathematical Development 12
2.1 Solution to the 1D Ambipolar Diffusion Equation 12
2.2 Special Cases 14
2.3 Simple approximation to the depletion current for an abrupt change in carrier lifetime 16
3 Abrupt (Heaviside function) decrease (or increase) in minority carrier lifetime with $g(x,t) = g(t)$ 19
3.1 Case where $g(x,t)$ is a step function, i.e. $g(x,t) = g_0, t > 0$ 20
3.2 Case where $g(x,t)$ is a square pulse 22
3.3 Case where $g(x,t)$ is a piecewise linear pulse 23
4 Example Problems 28
4.1 The heavily doped pn diode, no ohmic field 28
4.2 The lightly doped pn diode with an ohmic field 34
4.3 A lightly doped pn diode, J_p with $g(x,t) = g(t)$ piecewise-linear 34
5 Convergence and computing time considerations 37
6 Conclusions 44

Figures

1 Reverse biased pn diode under light or ionizing irradiation 10
2 Piecewise linear gamma irradiation with a neutron pulse at $t = t'$ 24
3 Photocurrent density due to a gamma square-wave irradiation with a concurrent neutron pulse. 30
4 Photocurrent density due to a gamma square-wave irradiation with a neutron pulse during recovery. 31
5 Excess minority carrier density as a function of x and t in the irradiated undepleted n-type region of a pn diode. 32
6 Excess minority carrier density as a function of x and t in the irradiated undepleted n-type region of a pn diode. 33
7 Photocurrent density due to a gamma square-wave irradiation with a concurrent neutron pulse and including the effect of an ohmic field, $E_n = -20$ V/cm. 34
8 Photocurrent density due to a piecewise-linear gamma irradiation with a non-concurrent neutron pulse and including the effect of an ohmic field, $E_n = -20$ V/cm. 36
9 Minority carrier current density convergence for the raw solution as a function of the number or terms, n, used in the raw Fourier sine series for the case of no ohmic field. 40
10 Minority carrier current density convergence for the raw solution as a function of the number or terms, n, used in the raw Fourier sine series for the case of a high ohmic field. 41
11 Minority carrier current density convergence for a high ohmic field using the highly convergent, partial closed form solution. 42
12 Minority carrier current density versus time from the undepleted n-doped region of an np diode for a negative ohmic field (top) and no ohmic field (bottom) using the partial closed form solution. 43

Tables

1 Definition and description of important physical constants and parameters. . . 18
2 Description of parameters used in the lightly doped piecewise-linear pn diode simulation. 35
3 Comparison of CPU times for the raw and partial closed form solutions as a function of number of Fourier terms for piecewise-linear pn diode simulations. 41

1 Introduction

Advanced numerical device simulators, capable of simulating non-linear and multi-dimensional transient drift/diffusion carrier movement and the resulting photocurrents have been developed over the last two decades ([2], [3], [4]). These calculations, however, may require hours of compute time on powerful machines and may not be easily incorporated into device simulators used by chip designers, such as SPICE [1] or XYCE [5], which may require calculations for thousands of devices in order to analyze the effect of photocurrents generated in a single chip. One application of circuit codes is the investigation of the response of microelectronic devices to ionizing radiation. Ionizing radiation produces a transient photocurrent in a semiconductor device. When the radiation source consists of neutrons or heavy ions, significant damage may occur in the crystalline structure, affecting the material properties of the device.

The transport behavior of excess carriers in semiconductors is described by the current and continuity equations for electrons and holes, as well as Poisson's equation, which relates the electric field and net charge density. For each carrier, the current equation may be substituted into the continuity equation, resulting in three equations describing carrier transport (pp. 320-327, [6]). The three resulting equations are not amenable to exact analytic mathematical analysis. The electrical neutrality or charge balance approximation suggested by Van Roosbroeck [7] is used to combine the electron and hole current-continuity equations into the single ambipolar diffusion equation (pp. 327-328 [6]). The electrical neutrality approximation states that the excess electron and hole densities are equal everywhere within the device. The parameters of the resulting approximate equation are the ambipolar diffusion parameters, as described in Table 1. The electric field in the ambipolar diffusion equation includes an external field imposed by a voltage bias applied at the device contacts and an internal field set up by the charged particles within the device. In many applications the internal electric field is small and may be ignored (see pp. 330-333, [6]). We make this assumption in this report. We will investigate the range over which the ambipolar diffusion equation accurately describes the three equation system in a future SAND report.

One of the most important components in an integrated circuit (IC) is the reverse biased *pn* (or *np*) diode. Since, under normal operating conditions, the leakage current from this component is minute, a large radiation-generated photocurrent has the potential to upset the entire IC. Figure 1 shows a reverse biased *pn* diode under light or ionizing radiation. We assume ohmic contacts at the device ends. In order to obtain an analytical solution for the photocurrents generated in such a device, we will consider it to consist of three segments; the undepleted n-doped region, the depleted region, and the undepleted p-doped region. We assume that the boundaries for these regions do not change with respect to time; a reasonable assumption if the carrier-generation rate is not too high (the radiation-generated excess carrier density is small compared to the majority excess carrier density at equilibrium). The lengths, L_1 and L_2 of the undepleted regions as well as the width of the depleted zone W may be determined analytically (see pg. 401 [6], for example). The local coordinates are taken for convenience in the mathematical analysis. The function $g(x,t)$ describes the excess carriers generated by irradiation in each of the three sections of the device. The current for the entire device consists of the sum of the depletion zone current

with the two minority carrier diffusion currents from the undepleted regions [8]. It may be expressed,

$$J_{total}(t) = J_p(t) + J_{depl}(t) + J_n(t) \tag{1}$$

Using the above assumptions, analytic solutions to the ambipolar diffusion equation for the photocurrent response to irradiated 1D *pn* junction diodes have been developed over the past four decades ([8],[9],[10],[11],[12],[13]). These photocurrent solutions are applicable under limited boundary conditions with restrictions on the carrier generation rate. An early transient radiation effects model is that of Wirth-Rogers [8], which describes the current density solution to the ambipolar diffusion equation for a semi-infinite 1D *pn* junction diode with no ohmic field in the undepleted region. Stuetzer [11] examined the steady state behavior of a diode under radiation and found the excess carrier and current densities for a

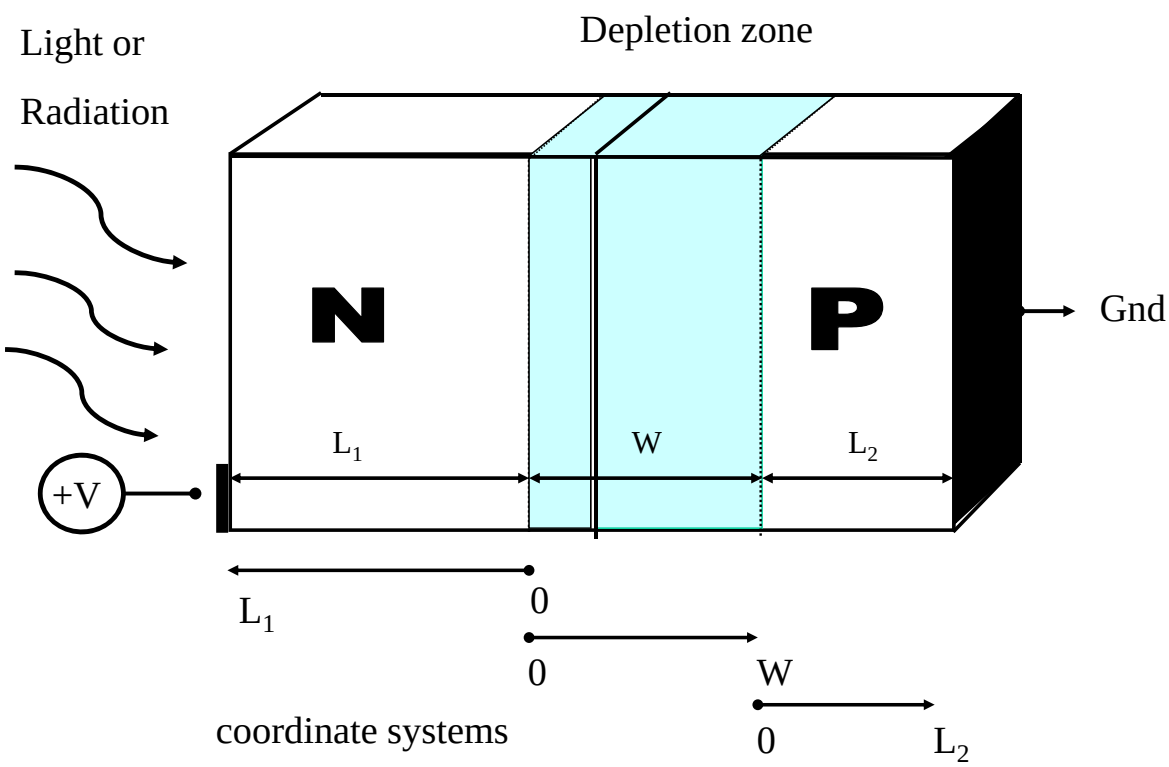

Figure 1: Reverse biased *pn* diode under light or ionizing irradiation. Device is irradiated from the left. For the 1D analysis, the contacts are assumed to cover the entire left and right hand surfaces. The shaded region represents the depletion zone and the unshaded regions represent undepleted zones. The total current is the sum of the drift and diffusion current from the depleted and undepleted zones. Local coordinate systems are shown. The parameter L in the mathematical development corresponds to either L_1 or L_2 in the figure.

diode of finite extent. A model by Enlow and Alexander [12] investigated the time-dependent solution of a finite *pn* junction diode irradiated by a square radiation pulse. They considered the effect of a constant ohmic field in the undepleted region, but the solution obtained was inaccurate due a poor approximation made in the Laplace transform inversion. The work of Wunsch and Axness [13] corrected that of Enlow and Alexander [12] by finding the exact inverse transform and also generalized and examined the limiting behavior of this solution. Work by Axness, Kerr, and Wunsch [9] extended the solution to monochromatic light pulses and found an n-dimensional transformation from the ADE to the non-homogeneous heat equation. This work suggested the use of finite Fourier sine transforms to solve problems involving the ADE. This SAND report generalizes the solutions of [9] to the particular case where there is a time-dependent change in the carrier lifetime during or after irradiation. Such behavior might be expected for a neutron pulse that is not coincident with a gamma irradiation of the device.

The effect of neutron damage to semiconductor devices has been studied by a number of authors ([14],[15],[16], [17]). Neutrons and other high energy particles collide and displace lattice atoms in semiconductors creating Frenkel defects. Primary displaced atoms typically have enough energy to create secondary defects. These vacancies may combine with dopant and impurity atoms to form stable defects, which, in turn, may serve as recombination centers, decreasing carrier lifetime. The temporal response of the carrier lifetime to a neutron burst has been characterized as an abrupt decrease followed by a rapid short-term anneal (on the order of a few hours) and a long-term anneal (on the order of months), in which the carrier lifetime increases ([14], [15], [18], [19]). Because the time scales associated with the annealing periods following a neutron pulse are very long in comparison to the length of a typical high-energy radiation (gamma) pulse, only an abrupt change in carrier lifetime is considered in this report. However, the general development of the next section allows an arbitrary time-dependent form of carrier lifetime.

The dynamics of neutron irradiation imply that the lattice damage and carrier lifetime degradation could be spatially-dependent. To our knowledge there is not a mathematical model describing this dependence. The analysis of this report assumes a spatially uniform carrier lifetime degradation, however, it may be possible to modify the analysis to a simple form of a spatially dependent lifetime. We do consider the possible spatial dependence of the excess carrier generation density in the following section. The resulting equations may be used to analyze the effects of a neutron irradiation on an abrupt *pn* junction illuminated by monochromatic light, for example.

2 Mathematical Development

In this section of the paper we develop general solutions to the excess carrier and current densities in the depleted and undepleted regions of a reverse biased pn diode.

2.1 Solution to the 1D Ambipolar Diffusion Equation

In Cartesian coordinates under the assumption of charge neutrality and a time-dependent carrier lifetime, the one-dimensional ambipolar diffusion equation may be written as ([6],[7]),

$$u_t = D_a u_{xx} - \mu_a E u_x - \frac{1}{\tau_a(t)} u + g(x,t) \qquad , \qquad 0 \leq x \leq L \qquad , \qquad t > 0 \tag{2}$$

where $u(x,t)$ is the excess carrier density, and $g(x,t)$ is the excess carrier generation rate (in excess of the thermal carrier generation rate). The equations for the ambipolar coefficients, D_a and μ_a and $\tau_a(t)$ are given in Table 1. E is the electric field, composed of an internal field due to internal charged carriers and an applied field due to an applied potential. The ambipolar carrier lifetime $\tau_a(t)$ is assumed a function of time in the analysis of this report. We assume that the degradation is spatially uniform throughout the device. We could investigate non-uniform lifetime degradation, but the spatial dependence in the PDE would then complicate the solution considerably. Inherent in the derivation of the ambipolar diffusion equation under the charge neutrality assumption, is the inference that both the minority and majority carrier lifetimes are affected equally with respect to time. Specifically, equation (10.2-29) of reference [6], becomes:

$$\frac{u}{\tau_a(t)} = \frac{p_0 + u}{\tau_p(t)} - \frac{p_0}{\tau_{p_0}} = \frac{n_0 + u}{\tau_n(t)} - \frac{n_0}{\tau_{n_0}} \tag{3}$$

where τ_{p_0} and τ_{n_0} are the average hole and electron carrier lifetimes respectively, under pre-irradiation thermal equilibrium conditions. For low-level carrier injection, $u(x,t)$ is much less than the majority carrier doping for the device and the ambipolar coefficients became approximately those of the minority carrier.

Thus, for an n-type device under low-level irradiation, D_a, μ_a, and $\tau_a(t)$ become D_p, μ_p, and $\tau_p(t)$, respectively. We assume the boundary conditions,

$$u(0,t) = u(L,t) = 0. \tag{4}$$

with the initial condition $u(x,0) = f(x)$. Under these conditions, the dominant current component in the undepleted n-type or p-type region of an np diode is the minority carrier

current. Its current density is given by [6],

$$J(t) = \left[qD\frac{\partial u}{\partial x} \pm qu\mu E \right]\Bigg|_{x=0} \tag{5}$$

where $\pm$ is positive for the computation of J_p in n-type material and negative for the computation of J_n in p-type material. The leading sign on the right-hand side of the above equation is chosen positive so that $J_p(t)$ is positive in our analysis. From this point on, we further simplify our analysis by dropping the p subscript from D_p, μ_p, and $\tau_p(t)$. We can solve the above boundary value problem via the substitution $u(x,t) = V(x,t)e^{ax}$, which will transform equation (2) to

$$V_t = DV_{xx} - (Da^2 + \frac{1}{\tau(t)})V + g(x,t)e^{-ax} \tag{6}$$

where $a = \frac{\mu E}{2D}$. The transformed boundary conditions remain type I, homogeneous, while the initial condition becomes $V(x,0) = f(x)e^{-ax}$. The resultant boundary value problem may be solved by the finite Fourier sine transform [21]. That is, define

$$\bar{V}_n(t) = \int_0^L V(x,t)\sin(\alpha_n x)dx \tag{7}$$

with inversion formula

$$V(x,t) = \frac{2}{L}\sum_{n=1}^{\infty}\bar{V}_n(t)\sin(\alpha_n x) \tag{8}$$

in which $\alpha_n = \frac{n\pi}{L}$ is the nth eigenvalue associated with the Fourier series for $V(x,t)$.

Applying this transform to equation (6), yields the ODE:

$$\frac{d}{dt}\bar{V}_n(t) + \left[D(\alpha_n^2 + a^2) + \frac{1}{\tau(t)} \right]\bar{V}_n(t) = \bar{G}_n(t) \qquad , \qquad n = 1,2,3... \tag{9}$$

in which

$$\bar{G}_n(t) = \int_0^L g(x,t)e^{-ax}\sin(\alpha_n x)dx \tag{10}$$

Applying the transform to the initial condition simply provides us with the initial condition for our ODE:

$$\bar{V}_n(0) = \int_0^L f(x)e^{-ax}\sin(\alpha_n x)dx$$

Therefore, the solution of our ODE is given by

$$\bar{V}_n(t) = \bar{V}_n(0)e^{-D(\alpha_n^2+a^2)t-\int_0^t \frac{1}{\tau(s)}ds} + \int_0^t \bar{G}_n(w)e^{-D(\alpha_n^2+a^2)(t-w)-\int_w^t \frac{1}{\tau(s)}ds}dw \tag{11}$$

Substituting equation (11) into equation (8) we obtain $V(x,t)$. Therefore

$$\begin{aligned} u(x,t) &= \frac{2e^{ax}}{L}\sum_{n=1}^{\infty}\left[\bar{V}_n(0)e^{-D(\alpha_n^2+a^2)t-\int_0^t \frac{1}{\tau(s)}ds}\right. \\ &+ \left.\int_0^t \bar{G}_n(w)e^{-D(\alpha_n^2+a^2)(t-w)-\int_w^t \frac{1}{\tau(s)}ds}dw\right]\sin(\alpha_n x) \end{aligned} \tag{12}$$

Equation (12) represents the general solution for the excess carrier density within the undepleted n-type region of the device. The corresponding current density evaluated at $x = 0$ is,

$$J_p(t) = \frac{2qD}{L}\sum_{n=1}^{\infty}\alpha_n\left[\bar{V}_n(0)e^{-D(\alpha_n^2+a^2)t-\int_0^t \frac{1}{\tau(s)}ds} + \int_0^t \bar{G}_n(w)e^{-D(\alpha_n^2+a^2)(t-w)-\int_w^t \frac{1}{\tau(s)}ds}dw\right] \tag{13}$$

The expressions given by equations (12) and (13) may be used to describe the excess carrier and current densities in the undepleted p-type region with appropriate subscript changes in the parameters and a possible sign change on the ohmic field term, depending on the axis orientation. The expressions given by equations (12) and (13) may be used to evaluate the excess carrier and current density distributions for an arbitrary function $\tau(s)$. In the case where the initial excess carrier density is zero at time $t = 0$, $\bar{V}_n(0) = 0$ and the first term is eliminated in the expressions. However, we note that the first term gives us a number of options in simulation. For example, we may stop a simulation and restart using the excess carrier density at the stopping time as the initial excess carrier density upon restart. Using this option, we may change parameters after stopping to approximate in a piecewise linear fashion non-linear problems in which parameters change with respect to time. With careful consideration of charge conservation and changes in the depletion region, we may approximate moving boundary problems resulting from device bias changes during irradiation, for example.

2.2 Special Cases

For the case of $g(x,t) = g(x)$ and $f(x) = 0$ equation (12) reduces to

$$u(x,t) = \frac{2e^{ax}}{L}\sum_{n=1}^{\infty}\bar{G}_n\left[\int_0^t e^{-D(\alpha_n^2+a^2)(t-w)-\int_w^t \frac{1}{\tau(s)}ds}dw\right]\sin(\alpha_n x) \tag{14}$$

and from equation (13),

$$J_p(t) = \frac{2qD}{L}\sum_{n=1}^{\infty}\bar{G}_n\alpha_n\left[\int_0^t e^{-D(\alpha_n^2+a^2)(t-w)-\int_w^t \frac{1}{\tau(s)}ds}dw\right] \tag{15}$$

in which

$$\bar{G}_n = \int_0^L g(x)e^{-ax}\sin(\alpha_n x)dx \tag{16}$$

For the case where $g(x,t) = g(t)$ and $f(x) = 0$ equation (12) reduces to

$$u(x,t) = \frac{2e^{ax}}{L}\sum_{n=1}^{\infty}\bar{w}_n\left[\int_0^t g(w)e^{-D(\alpha_n^2+a^2)(t-w)-\int_w^t \frac{1}{\tau(s)}ds}dw\right]\sin(\alpha_n x) \tag{17}$$

in which

$$\bar{w}_n = \int_0^L e^{-ax}\sin(\alpha_n x)dx = \frac{\alpha_n\left(1-(-1)^n e^{-aL}\right)}{a^2+\alpha_n^2} \tag{18}$$

From equation (13), we find

$$J_p(t) = \frac{2qD}{L}\sum_{n=1}^{\infty}\bar{w}_n\alpha_n\left[\int_0^t g(w)e^{-D(\alpha_n^2+a^2)(t-w)-\int_w^t \frac{1}{\tau(s)}ds}dw\right]. \tag{19}$$

When $E = 0$, and therefore, $a = 0$, $\bar{w}_n = 0$ for n even and $\bar{w}_n = 2/\alpha_n$ for n odd. Therefore, equations (17) and (19) become,

$$u(x,t) = \frac{4}{L}\sum_{n=0}^{\infty}\left[\int_0^t g(w)e^{-D\alpha_{2n+1}^2(t-w)-\int_w^t \frac{1}{\tau(s)}ds}dw\right]\frac{\sin(\alpha_{2n+1}x)}{\alpha_{2n+1}} \tag{20}$$

and

$$J_p(t) = \frac{4qD}{L}\sum_{n=0}^{\infty}\int_0^t g(w)e^{-D\alpha_{2n+1}^2(t-w)-\int_w^t \frac{1}{\tau(s)}ds}dw. \tag{21}$$

From the above forms we note that when $E = 0$, any of the solutions that follow may be re-indexed to sum over only the odd terms, replacing the $\bar{w}_n$ term with $1/\alpha_{2n+1}$ and multiplying the leading coefficient of the series by a factor of 2.

2.3 Simple approximation to the depletion current for an abrupt change in carrier lifetime

In this section we derive an approximate expression for the depletion current density, $J_{depl}(t)$, due to a radiation source, taking into account an abrupt change in the carrier lifetime. The expression is a generalization to that derived in reference [9]. We make the following assumptions in the depleted region:

- The effective electric field is the sum of the applied and built-in field. This field is approximately constant and is unaffected by excess carriers (low-level radiation assumption).
- Except for electron-hole recombination, the effect of carrier-carrier interactions is negligible.
- Electron-hole pairs are instantaneously created by irradiation and instantaneously accelerated to a common drift velocity.
- Diffusion is negligible.
- Carriers arriving at the edge of the depletion region instantaneously contribute to the device current.
- The carrier lifetime is piecewise constant; $\tau(t) = \tau_1$ until time t' at which it becomes $\tau(t) = \tau_2$

Under these conditions, the drift velocity is $v = dx/dt = \mu E$. For E negative, electrons move toward the origin and a carrier arriving at the depletion edge ($x = 0$ in Figure (1)) at time t was originally generated from the position $x^* \geq 0$ at time $t - t^* = t - x^*/(\mu |E|)$. For an irradiation that begins at time $t = 0$, carriers generated with flux $g(x^*, t - x^*/(\mu |E|))$ located a distance $x^* \leq \min(\mu |E| t, W)$ contribute to the photocurrent.

We consider the effect of carrier recombination in the depleted region. When $t^* \leq t < t'$, on average, the fraction $\exp(-t^*/\tau_1) = \exp[-x^*/(\mu |E| \tau_1)]$ of the originally injected carriers at position $x = x^*$ reach the depletion edge.

When $t \geq t^* \geq t'$, particles in the spatial interval, $[0, \min(\mu |E| (t - t'), W)]$ travel to the depletion edge in the time interval $[t', t]$, corresponding to the carrier lifetime, τ_2. In this interval, on average the fraction $\exp(-t^*/\tau_2) = \exp[-x^*/(\mu |E| \tau_2)]$ of the originally injected carriers reach the depletion edge. Particles generated in the spatial interval, $[\min(\mu |E| (t - t'), W), \min(\mu |E| t, W)]$, travel under carrier lifetime τ_1 during the interval $[t - t^*, t']$ and under carrier lifetime τ_2 over the interval $[t', t]$.

Considering the average arrival time of carriers, that each carrier has a charge of q, and the relative times that the carriers travel under each recombination rate, the photocurrent

density may be written,

$$J_{depl}\left(t\right)=\begin{cases} q\int_{0}^{\min(\mu|E|t,W)} g\left(x^{*},t-x^{*}/\left(\mu\left|E\right|\right)\right)e^{-x^{*}/(\mu|E|\tau_{1})}dx^{*}, & t<t' \\ q\int_{0}^{\min(\mu|E|(t-t'),W)} g\left(x^{*},t-x^{*}/\left(\mu\left|E\right|\right)\right)e^{-x^{*}/(\mu|E|\tau_{2})}dx^{*}+ & \\ q\int_{\min(\mu|E|(t-t'),W)}^{\min(\mu|E|t,W)} g\left(x^{*},t-x^{*}/\left(\mu\left|E\right|\right)\right)e^{-(x^{*}-x')/(\mu|E|\tau_{1})}e^{-x'/(\mu|E|\tau_{2})}dx^{*}, & t\geq t' \end{cases} \tag{22}$$

where $x'=\mu\left|E\right|t'$. The first integral in the expression for $t\geq t'$ represents the contribution of carriers that have been generated after the neutron pulse and the second integral represents the contribution of carriers that have been generated before the neutron pulse. The *min* function in the integral limits the charge collection to be from the interval $[0,W]$. Note that for t large enough, the first integrals will span the entire range $[0,W]$ and the second integral of the expression for $t\geq t'$, becomes identically zero. For a radiation source, $g\left(x,t\right)$ is normally a function of t only. For $g(t)=g_{0}(t>0)$ and a finite carrier lifetime, the above expression may be evaluated as:

$$J_{depl}\left(t\right)=\begin{cases} qg_{0}\mu\left|E\right|\tau_{1}\left(1-e^{-\min(t/\tau_{1},W/(\mu|E|\tau_{1}))}\right), & t<t' \\ qg_{0}\mu\left|E\right|\tau_{2}\left(1-e^{-\min((t-t')/\tau_{2},W/(\mu|E|\tau_{2}))}\right)+ & \\ qg_{0}\mu\left|E\right|\tau_{1}e^{-t'(1/\tau_{2}-1/\tau_{1})}. & \\ \left(e^{-\min((t-t')/\tau_{1},W/(\mu|E|\tau_{1}))}-e^{-\min(t/\tau_{1},W/(\mu|E|\tau_{1}))}\right), & t\geq t' \end{cases} \tag{23}$$

Table 1: Definition and description of important physical constants and parameters.

Constant	**Description**	**Units**
G	generation density per rad/s in Si (4.3×10^{13})	$1/\text{cm}^3/\text{rad(Si)}$
q	Electronic charge (1.602×10^{-19})	C
k	Boltzmann constant (1.381×10^{-23})	J/K
Parameter	**Description/Equation**	**cgs units**
a	$\mu_p E_n / 2D_p$	1/cm
E, E_p, E_n	Ohmic electric field in undepleted zone	V/cm
$J(t), J_{p \text{ or } n}(t)$	Undepleted zone current densities	A/cm^2
$n\,(x,t)$	electrons per unit volume	$1/\text{cm}^3$
$p\,(x,t)$	holes per unit volume	$1/\text{cm}^3$
$u\,(x,t)$	$n\,(x,t) - n\,(x,0)$, Excess electrons/unit volume	$1/\text{cm}^3$
$u\,(x,t)$	$p\,(x,t) - p\,(x,0)$, Excess holes/unit volume	$1/\text{cm}^3$
τ_p, τ_n	Minority carrier lifetime	s
τ_1	minority carr. lifetime before neutron pulse	s
τ_2	minority carr. lifetime after neutron pulse	s
μ_p, μ_n	Minority carrier mobility	cm^2/Vs
D, D_p, D_n	Minority carrier diffusion coefficient	cm^2/s
D_a	$\frac{(n+p)D_n D_p}{nD_n + pD_p}$ Ambipolar diffusion	cm^2/s
μ_a	$\frac{(n_0 - p_0)\mu_n \mu_p}{n\mu_n + p\mu_p}$ Ambipolar mobility	cm^2/Vs
τ_a	$\frac{p_0+u}{\tau_p(t)} - \frac{p_0}{\tau_{p0}} = \frac{n_0+u}{\tau_n(t)} - \frac{n_0}{\tau_{n0}}$ Ambipolar lifetime	s
L_p, L_n	$\sqrt{D_p \tau_p}$, $\sqrt{D_n \tau_n}$, Diffusion length	cm
L	undepleted p or n width	cm
W	depletion width	cm
$\dot{\gamma}$	dose rate	rad(Si)/s
$g\,(x,t)$, g_0	G $\dot{\gamma}$, generation density	$1/\text{cm}^3\text{s}$
α_n	$n\pi/L$, Fourier sine series eigenvalue	1/cm
$a_{i,n}$	$D(\alpha_n^2 + a^2 + \frac{1}{D\tau_i})$ sine series parameter	1/s
Dimensionless parameters [9]	**Description**	**Definition**
a_k	solution parameter, n-type region	$\left(\frac{k\pi}{\zeta_p}\right)^2 + 1 + \beta_p^2$
b_k	solution parameter, p-type region	$\left(\frac{k\pi}{\zeta_n}\right)^2 + 1 + \beta_n^2$
ζ_p, ζ_n	Normalized diode length	$\frac{x_1}{L_p}, \frac{x_2}{L_n}$
β_p, β_n	Normalized field parameter	$\frac{\mu_p E_n L_p}{2D_p}$, $\frac{\mu_n E_p L_n}{2D_n}$
t_p, t_n	Normalized time	$\frac{t}{\tau_p}$, $\frac{t}{\tau_n}$
δt_p, δt_n	Normalized pulse length	$\frac{\delta t}{\tau_p}$, $\frac{\delta t}{\tau_n}$

3 Abrupt (Heaviside function) decrease (or increase) in minority carrier lifetime with $g(x,t) = g(t)$

In this section we investigate the effect of an abrupt change in minority carrier lifetime during or after a time-dependent spatially-uniform gamma irradiation pulse, $g(x,t) = g(t)$. A typical application is that of a neutron burst which may result in a decrease of carrier lifetime of an order of magnitude or more. The mathematical analysis is also applicable to an abrupt increase in minority carrier lifetime since the value assigned to the lifetime after the abrupt change may be greater or less than the initial carrier lifetime in the equations. The solution to the problem for a constant minority carrier lifetime (i.e. no neutron pulse) is known [9].

Assuming the minority carrier lifetime is characterized as; $\tau(t) = \tau_1$, $t \leq t'$ and $\tau(t) = \tau_2$, $t > t'$, the integral in the exponential terms of the equations of the previous section (i.e. (14),(15),(17), or (19)) becomes,

$$\int_w^t \frac{1}{\tau(s)} ds = \begin{cases} \frac{t-w}{\tau_1} & , \quad t \in [0, t') \\ \frac{t'-w}{\tau_1} + \frac{t-t'}{\tau_2} & , \quad t \in [t', \infty), w \in [0, t') \\ \frac{t-w}{\tau_2} & , \quad t \in [t', \infty), w \in [t', \infty) \end{cases} \tag{24}$$

so that,

$$u(x,t) = \frac{2e^{ax}}{L} \sum_{n=1}^{\infty} \bar{w}_n I_n(t) \sin(\alpha_n x) \tag{25}$$

and from equation (19),

$$J_p(t) = \frac{2qD}{L} \sum_{n=1}^{\infty} \bar{w}_n \alpha_n I_n(t) \tag{26}$$

where

$$I_n(t) = \begin{cases} I_{1,n}(0,t); & 0 \leq t \leq t' \\ e^{-a_{2,n}(t-t')} I_{1,n}(0,t') + I_{2,n}(t',t); & t > t' \end{cases} \tag{27}$$

and,

$$I_{k,n}(a,b) = \int_a^b g(w) e^{-a_{k,n}(b-w)} dw, \tag{28}$$

in which $a_{k,n} = D(\alpha_n^2 + a^2 + \frac{1}{D\tau_k})$. In the following sections we evaluate $I_n(t)$ using equations (27) and (28) for specific cases of $g(t)$. We then evaluate $u(x,t)$ and $J_p(t)$ using equations (25) and (26).

3.1 Case where $g(x,t)$ is a step function, i.e. $g(x,t) = g_0, t > 0$

In this case, evaluation of equation (27) gives,

$$I_n(t) = \begin{cases} \frac{g_0(1-e^{-a_{1,n}t})}{a_{1,n}} & , \quad 0 < t \leq t' \\ \frac{g_0(1-e^{-a_{1,n}t'})}{a_{1,n}} e^{-a_{2,n}(t-t')} + \frac{g_0(1-e^{-a_{2,n}(t-t')})}{a_{2,n}} & , \quad t' < t \end{cases} \tag{29}$$

where $a_{1,n}$ and $a_{2,n}$ are defined in section 3. Substitution of the above formula into either equation (25) or equation (26) provide us with the relevant solutions. The convergence rates of the two respective raw series may, however, be significantly improved by decomposing them into steady-state and transient components, and then replacing the steady-state series with the appropriate closed-form formulas given in Appendix A. The solution for $u(x,t)$ may then be written,

$$u(x,t) = \begin{cases} u_{s,1}(x) - \frac{2g_0 e^{ax}}{L} \sum_{n=1}^{\infty} \bar{w}_n \frac{e^{-a_{1,n}t}}{a_{1,n}} \sin(\alpha_n x) & , \quad 0 < t \leq t' \\ u_{s,2}(x) + \frac{2g_0 e^{ax}}{L} \sum_{n=1}^{\infty} \bar{w}_n \left[\frac{1-e^{-a_{1,n}t'}}{a_{1,n}} e^{-a_{2,n}(t-t')} - \frac{e^{-a_{2,n}(t-t')}}{a_{2,n}} \right] \sin(\alpha_n x) & , \quad t' < t \end{cases} \tag{30}$$

where

$$u_{s,k}(x) = g_0 \tau_k \left[1 - e^{ax} \frac{\left(\sinh(\gamma_k(L-x)) + e^{-aL}\sinh(\gamma_k x)\right)}{\sinh(\gamma_k L)} \right]. \tag{31}$$

Applying the same technique to equation (26) using equation (29), we have,

$$J_p(t) = \begin{cases} J_{s,1} - \frac{2qDg_0}{L}\sum_{n=1}^{\infty}\bar{w}_n\alpha_n\frac{e^{-a_{1,n}t}}{a_{1,n}} & , \quad 0 < t \leq t' \\ \\ J_{s,2} + \frac{2qDg_0}{L}\sum_{n=1}^{\infty}\bar{w}_n\alpha_n\left[\frac{1-e^{-a_{1,n}t'}}{a_{1,n}}e^{-a_{2,n}(t-t')} - \frac{e^{-a_{2,n}(t-t')}}{a_{2,n}}\right] & , \quad t' < t \end{cases} \tag{32}$$

in which

$$J_{s,k} = qDg_0\tau_k\left[-a + \gamma_k\frac{\left(\cosh(\gamma_k L) - e^{-aL}\right)}{\sinh(\gamma_k L)}\right] \tag{33}$$

The terms $u_{s,k}(x)$ and $J_{s,k}$ represent the steady state minority excess carrier and current densities with respect to the initial ($k = 1$) and final ($k = 2$) minority carrier densities. We note that the equations (30) and (32) agree with equations (18) and (19) of Axness et. al. [9], for the case where there is no change in carrier lifetime ($\tau_1 = \tau_2$). We may write the above in the notation of equations (20) and (21) of Axness et. al. [9] as (see Appendix A),

$$J_p(t) = \begin{cases} J_{p,1}(\infty) - A_{p,1}\sum_{n=1}^{\infty}\frac{(n\pi)^2\left(1-(-1)^n e^{-\zeta_{p,1}\beta_{p,1}}\right)}{(n\pi)^2+(\zeta_{p,1}\beta_{p,1})^2}\left[\frac{e^{-a_{n,1}t_{p,1}}}{a_{n,1}}\right] & , \quad t \in [0, t_1) \\ \\ J_{p,2}(\infty) - A_{p,1}\sum_{n=1}^{\infty}\frac{(n\pi)^2\left(1-(-1)^n e^{-\zeta_{p,1}\beta_{p,1}}\right)}{(n\pi)^2+(\zeta_{p,1}\beta_{p,1})^2}\cdot \\ \left[\frac{e^{(t_{p,2}-t_{1,2})}\left(e^{-a_{n,1}t_{p,1}} - e^{-d_{p,1}(t_{p,1}-t_{1,1})}\right)}{a_{n,1}} + \frac{\tau_{p,2}e^{-a_{n,2}(t-t_1)}}{\tau_{p,1}a_{n,2}}\right] & , \quad t \in [t_1, \infty) \end{cases}$$

with $d_{p,1} = \frac{n\pi}{\zeta_{p,1}} + \beta_{p,1}$ and

$$J_{p,k}(\infty) = qg_0L_{p,k}\left[\frac{\sqrt{(}1+\beta_{p,k}^2)\left[\cosh(\zeta_{p,k}\sqrt{(}1+\beta_{p,k}^2)) - e^{-\zeta_{p,k}\beta_{p,k}}\right]}{\sinh(\zeta_{p,k}\sqrt{1+\beta^2})} - \beta_{p,k}\right] \tag{34}$$

where the parameters are given in Table 1. The k in the above coefficients and in $J_{p,k}(\infty)$ refers to the notation of Axness et. al. [9] with τ_1 applied when $k = 1$ and τ_2 applied for $k = 2$. The subscript p refers to the minority carrier current in an n-doped device. The photocurrent for a p-doped device has the same formula with a sign change for the ohmic field term E.

3.2 Case where $g(x,t)$ is a square pulse

In this case, the carrier lifetime is that of the previous section. The excess carrier generation density is defined by $g(x,t) = g_0(1 - H(t - t_1))$, where $H(t)$ denotes the Heaviside function. For the case where the neutron pulse occurs during the gamma irradiation ($t' < t_1$), we may evaluate $I_n(t)$ using equation (27) as,

$$I_n(t) = \begin{cases} \frac{g_0\left(1-e^{-a_{1,n}t}\right)}{a_{1,n}} & , \quad 0 < t \leq t' \\ I_n(t')e^{-a_{2,n}(t-t')} + \frac{g_0\left(1-e^{-a_{2,n}(t-t')}\right)}{a_{2,n}} & , \quad t' < t \leq t_1 \\ I_n(t_1)e^{-a_{2,n}(t-t_1)} & , \quad t > t_1 \end{cases} \tag{35}$$

And for the case where the neutron pulse occurs after the gamma irradiation ($t' > t_1$), we may evaluate $I_n(t)$ using equation (27) as,

$$I_n(t) = \begin{cases} \frac{g_0\left(1-e^{-a_{1,n}t}\right)}{a_{1,n}} & , \quad 0 < t \leq t_1 \\ I_n(t_1)e^{-a_{1,n}(t-t_1)} & , \quad t_1 < t \leq t' \\ I_n(t')e^{-a_{2,n}(t-t')} & , \quad t > t' \end{cases} \tag{36}$$

where $a_{1,n}$ and $a_{2,n}$ are as defined in section 3. As expected, equation (35) is the same as equation (29) for the step function except over the interval $t > t_1$. We note that equation (36) over the range $t > t_1$ takes the form of $I_n(t)$ evaluated at the previous endpoint multiplied by an exponential term dependent upon the time elapsed since that endpoint. The terms, $a_{k,n}$, in the exponential argument represent the effective rate of carrier degradation for each eigenvalue taking into account losses through drift, diffusion, and recombination. This rate is dependent upon the minority carrier lifetime during which the elapsed time occurs ($k = 1$ for τ_1 and $k = 2$ for τ_2). Similar terms occur in equation (35). Here, over the range of $t' < t \leq t_1$, where the gamma pulse continues, the second term on the right hand side represents the contribution of excess carriers produced during this period. The final equation for $t > t_1$, has the same form as equation (36). Finally, we note that partial closed form solutions for $u(x,t)$ and $J_p(t)$ may be obtained as in section 3.1. The development is given in Appendix

A and the results for $t' < t_1$ are,

$$u(x,t) = \begin{cases} u_{s,1}(x) - \frac{2g_0 e^{ax}}{L} \sum_{n=1}^{\infty} \bar{w}_n \frac{e^{-a_{1,n}t}}{a_{1,n}} \sin(\alpha_n x) & 0 < t \leq t' \\ u_{s,2}(x) + \frac{2g_0 e^{ax}}{L} \sum_{n=1}^{\infty} \bar{w}_n \left[\frac{1-e^{-a_{1,n}t'}}{a_{1,n}} e^{-a_{2,n}(t-t')} - \frac{e^{-a_{2,n}(t-t')}}{a_{2,n}} \right] \sin(\alpha_n x) & t' < t \leq t_1 \\ \frac{2g_0 e^{ax}}{L} \sum_{n=1}^{\infty} \bar{w}_n \left[\frac{1-e^{-a_{1,n}t'}}{a_{1,n}} e^{-a_{2,n}(t-t')} + \frac{1-e^{-a_{2,n}(t_1-t')}}{a_{2,n}} e^{-a_{2,n}(t-t_1)} \right] \sin(\alpha_n x) & t > t_1 \end{cases} \tag{37}$$

and

$$J_p(t) = \begin{cases} J_{s,1} - \frac{2qDg_0}{L} \sum_{n=1}^{\infty} \bar{w}_n \alpha_n \frac{e^{-a_{1,n}t}}{a_{1,n}} & 0 < t \leq t' \\ J_{s,2} + \frac{2qDg_0}{L} \sum_{n=1}^{\infty} \bar{w}_n \alpha_n \left[\frac{1-e^{-a_{1,n}t'}}{a_{1,n}} e^{-a_{2,n}(t-t')} - \frac{e^{-a_{2,n}(t-t')}}{a_{2,n}} \right] & t' < t \leq t_1 \\ \frac{2qDg_0}{L} \sum_{n=1}^{\infty} \bar{w}_n \alpha_n \left[\frac{1-e^{-a_{1,n}t'}}{a_{1,n}} e^{-a_{2,n}(t-t')} + \frac{1-e^{-a_{2,n}(t_1-t')}}{a_{2,n}} e^{-a_{2,n}(t-t_1)} \right] & t > t_1 \end{cases} \tag{38}$$

where $u_{s,k}(x)$ and $J_{s,k}$ are given by equations (31) and (33). These terms again represent the steady state current densities. The equations for the case where $t' > t_1$ are given in Appendix A.

3.3 Case where $g(x,t)$ is a piecewise linear pulse

Experiments conducted at high-energy facilities generally measure the radiation generation density. Typically, the function describing this pulse is not a square wave, but may easily be described by a piecewise linear function with respect to time, as shown in Figure 2. For the case where the neutron pulse occurs during the gamma irradiation, we may evaluate $I_n(t)$ using equation (27) as,

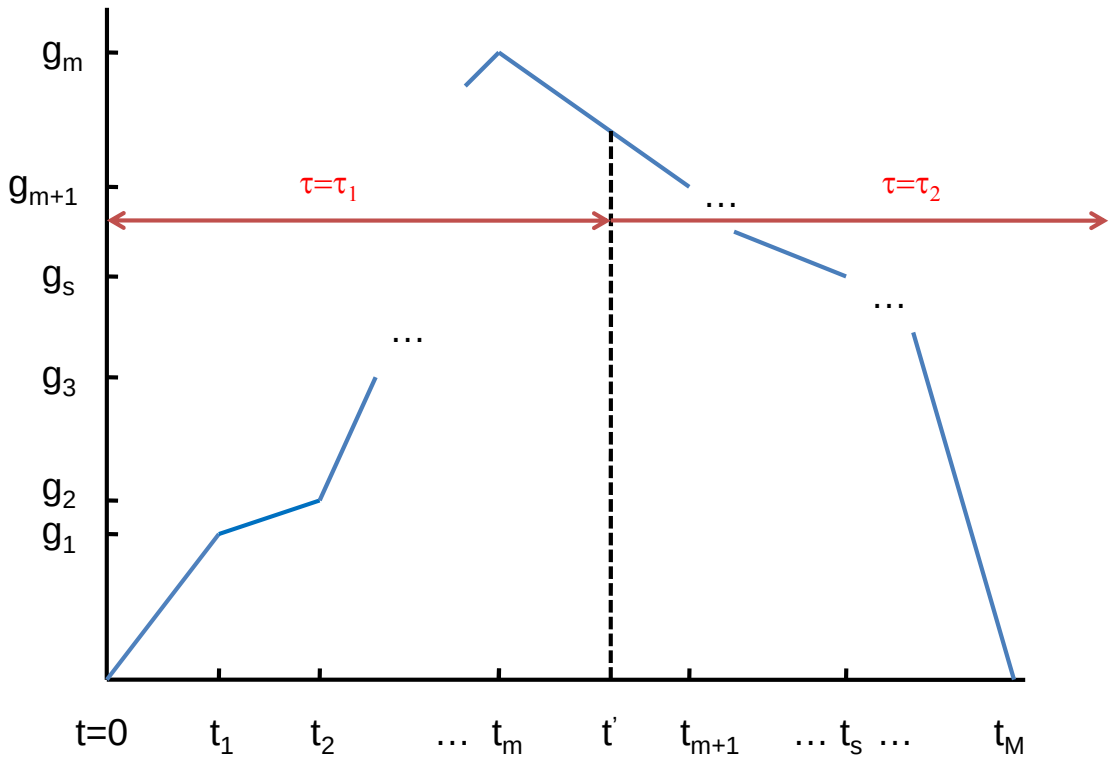

Figure 2: Piecewise linear gamma irradiation generation density with a neutron pulse at $t = t'$. *pn* diode minority carrier lifetime is $\tau = \tau_1$ for $t < t'$ and $\tau = \tau_2$ for $t \geq t'$.

$$
I_n(t) =
\begin{cases}
\sum_{i=0}^{m-1} \int_{t_i}^{t_{i+1}} \left[g_i + h_i\left(w - t_i\right)\right] e^{-a_{1,n}(t-w)} dw + \\
\int_{t_m}^{t} \left[g_m + h_m\left(w - t_m\right)\right] e^{-a_{1,n}(t-w)} dw & , \quad 0 \le t_m < t \le t' < t_{m+1} \\
\\
I_n(t') e^{-a_{2,n}(t-t')} + \\
\int_{t'}^{t} \left[g_m + h_m\left(w - t_m\right)\right] e^{-a_{2,n}(t-w)} dw & , \quad t_m \le t' < t \le t_{m+1} \\
\\
I_n(t_{m+1}) e^{-a_{2,n}(t-t_{m+1})} + \\
\sum_{i=m+1}^{s-1} \int_{t_i}^{t_{i+1}} \left[g_i + h_i\left(w - t_i\right)\right] e^{-a_{2,n}(t-w)} dw + \\
\int_{t_s}^{t} \left[g_s + h_s\left(w - t_s\right)\right] e^{-a_{2,n}(t-w)} dw & , \quad t_{m+1} < t_s < t \le t_{s+1} \le t_M \\
\\
I_n(t_M) e^{-a_{2,n}(t-t_M)} & , \quad t > t_M
\end{cases}
\tag{39}
$$

where $h_i = \frac{g_{i+1} - g_i}{t_{i+1} - t_i}$ is the slope of the ith line. Evaluating the integrals, and rearranging terms we find,

$$
I_n(t) =
\begin{cases}
\frac{1}{a_{1,n}} \left\{ \sum_{i=0}^{m-1} \left[\left(g_{i+1} - \frac{h_i}{a_{1,n}} \right) e^{-a_{1,n}(t-t_{i+1})} - \left(g_i - \frac{h_i}{a_{1,n}} \right) e^{-a_{1,n}(t-t_i)} \right] \right. \\
\left. + h_m\left(t - t_m\right) + \left(g_m - \frac{h_m}{a_{1,n}} \right) \left(1 - e^{-a_{1,n}(t-t_m)} \right) \right\}, & 0 \le t_m < t \le t' < t_{m+1} \\
\\
I_n(t') e^{-a_{2,n}(t-t')} + \frac{1}{a_{2,n}} \left\{ h_m\left(t - t'\right) + \right. \\
\left. \left(h_m\left(t' - t_m\right) + g_m - \frac{h_m}{a_{2,n}} \right) \left(1 - e^{-a_{2,n}(t-t')} \right) \right\}, & t_m \le t' < t \le t_{m+1} \\
\\
I_n(t_{m+1}) e^{-a_{2,n}(t-t_{m+1})} + \\
\frac{1}{a_{2,n}} \left\{ \sum_{i=m+1}^{s-1} \left[\left(g_{i+1} - \frac{h_i}{a_{2,n}} \right) e^{-a_{2,n}(t-t_{i+1})} - \left(g_i - \frac{h_i}{a_{2,n}} \right) e^{-a_{2,n}(t-t_i)} \right] \right. \\
\left. + h_s\left(t - t_s\right) + \left(g_s - \frac{h_s}{a_{2,n}} \right) \left(1 - e^{-a_{2,n}(t-t_s)} \right) \right\}, & t_{m+1} < t_s < t \le t_{s+1} \le t_M \\
\\
I_n(t_M) e^{-a_{2,n}(t-t_M)}, & t > t_M
\end{cases}
\tag{40}
$$

Alternatively, $I_n(t)$ may be written,

$$
I_n(t) = \begin{cases}
\frac{1}{a_{1,n}}\left\{h_0 t + \left(g_0 - \frac{h_0}{a_{1,n}}\right)\left(1 - e^{-a_{1,n}t}\right)\right\}, & 0 < t \leq t_1 \\
I_n(t_s)e^{-a_{1,n}(t-t_s)} + \frac{1}{a_{1,n}}\Big\{h_s\left(t - t_s\right) + & \\
\left(g_s - \frac{h_s}{a_{1,n}}\right)\left(1 - e^{-a_{1,n}(t-t_s)}\right)\Big\}, & t_s < t \leq t_{s+1} \\
 & (s \text{ such that } 1 \leq s < m) \\
I_n(t_m)e^{-a_{1,n}(t-t_m)} + \frac{1}{a_{1,n}}\Big\{h_m\left(t - t_m\right) + & \\
\left(g_m - \frac{h_m}{a_{1,n}}\right)\left(1 - e^{-a_{1,n}(t-t_m)}\right)\Big\}, & t_m < t \leq t' < t_{m+1} \\
I_n(t')e^{-a_{2,n}(t-t')} + \frac{1}{a_{2,n}}\Big\{h_m\left(t - t'\right) + & \\
\left(h_m\left(t' - t_m\right) + g_m - \frac{h_m}{a_{2,n}}\right)\left(1 - e^{-a_{2,n}(t-t')}\right)\Big\}, & t' < t \leq t_{m+1} \\
I_n(t_s)e^{-a_{2,n}(t-t_s)} + \frac{1}{a_{2,n}}\Big\{h_s\left(t - t_s\right) + & \\
\left(g_s - \frac{h_s}{a_{2,n}}\right)\left(1 - e^{-a_{2,n}(t-t_s)}\right)\Big\}, & t_s < t \leq t_{s+1} \\
 & (s \text{ such that } m+1 \leq s < M) \\
I_n(t_M)e^{-a_{2,n}(t-t_M)}, & t > t_M
\end{cases} \tag{41}
$$

The corresponding raw series for $u(x,t)$ and $J_p(t)$ may be written using closed form formulas for some of the terms (see Appendix A). This enables us to obtain a much faster convergence rate (see section 5). The partial closed form solutions may then be written,

$$u(x,t) = \frac{2e^{ax}}{L} \cdot$$

$$\begin{cases} [h_m(t-t_m)+g_m]\, S(x)_{1,1} \\ -h_m S(x)_{1,2} + \sum\limits_{n=1}^{\infty} \bar{w}_n R_n(t) \sin(\alpha_n x), & 0 \le t_m < t \le t' < t_{m+1} \\ \\ [h_m(t-t_m)+g_m]\, S(x)_{2,1} \\ -h_m S(x)_{2,2} + \sum\limits_{n=1}^{\infty} \bar{w}_n R_n(t) \sin(\alpha_n x), & t_m \le t' < t \le t_{m+1} \\ \\ [h_s(t-t_s)+g_s]\, S(x)_{2,1} \\ -h_s S(x)_{2,2} + \sum\limits_{n=1}^{\infty} \bar{w}_n R_n(t) \sin(\alpha_n x), & t_{m+1} < t_s < t \le t_{s+1} \le t_M \\ \\ \sum\limits_{n=1}^{\infty} \bar{w}_n R_n(t) \sin(\alpha_n x), & t > t_M \end{cases} \tag{42}$$

and

$$J_p(t) =$$

$$\frac{2qD}{L} \begin{cases} [h_m(t-t_m)+g_m]\, S_{1,1} \\ -h_m S_{1,2} + \sum\limits_{n=1}^{\infty} \bar{w}_n \alpha_n R_n(t), & 0 \le t_m < t \le t' < t_{m+1} \\ \\ [h_m(t-t_m)+g_m]\, S_{2,1} \\ -h_m S_{2,2} + \sum\limits_{n=1}^{\infty} \bar{w}_n \alpha_n R_n(t), & t_m \le t' < t \le t_{m+1} \\ \\ [h_s(t-t_s)+g_s]\, S_{2,1} \\ -h_s S_{2,2} + \sum\limits_{n=1}^{\infty} \bar{w}_n \alpha_n R_n(t), & t_{m+1} < t_s < t \le t_{s+1} \le t_M \\ \\ \sum\limits_{n=1}^{\infty} \bar{w}_n R_n(t) \sin(\alpha_n x), & t > t_M \end{cases} \tag{43}$$

with $S(x)_{i,j}$, $S_{i,j}$, and $R_n(t)$ given by equations (A-3)-(A-6) and (A-25) in Appendix A. Since the expression for $g(t)$ is general in the above derivation, we may also compute $u(x,t)$ and $J_p(t)$ for the case where $t' > t_M$ by employing equations (42) and (43) and by introducing an additional segment to Figure 2 upon which we define $g(t) = 0$ in the interval $t_M < t \le t' = t_{M+1}$.

4 Example Problems

In this section we present some example problems that illustrate the behavior of a *pn* diode that undergoes a neutron pulse both during and following a gamma irradiation. A neutron pulse produces an instantaneous reduction of the minority carrier lifetime in the *pn* diode, as illustrated in Figure 1 of [15]. These examples will illustrate the current and excess carrier density response to a gamma irradiation followed by a neutron pulse in the undepleted n-type region of the diode. Abrupt junction *pn* diodes both with and without constant ohmic fields in the undepleted n-type region will be examined. For our examples we use the parameters of Figures 2 and 3 in [9].

4.1 The heavily doped *pn* diode, no ohmic field

Note that we will use the subscript p in this section to denote the minority carrier in the n-type substrate. For our first example, we use the parameters of Figure 2 in [9] to examine the photocurrent response due to irradiation and a neutron pulse. Specifically, setting the minority carrier diffusion coefficient and the initial minority carrier lifetime to 11.31 cm^2/s and 2x10^{-5} s, respectively, the minority carrier diffusion length becomes $L_p = \sqrt{D_p \tau_p} =$ 0.015 cm. Setting $L = 0.0049$ cm, the parameter $\zeta_p = L/L_p = 0.32$ as in [9]. It is assumed that there is no ohmic field in the undepleted n-type region. A 1x10^9 rad(Si)/s square wave gamma pulse is assumed to begin at $t = 0$ and end at $t = 2.4$ μs. The gamma irradiation is assumed longer in this example than that of Figure 2 of reference [9] to illustrate the dual steady state photocurrent behavior imposed by the neutron pulse. The neutron pulse is assumed to cause an abrupt minority carrier lifetime degradation of from one to four orders of magnitude.

Figure 3 gives the analytic photocurrent density in the undepleted n-doped region, computed from equation (38) after the aforementioned gamma irradiation, where a neutron pulse occurs at $t = 1.5$ μs. The computation gives the analytic photocurrent density with respect to time. The top (solid) curve assumes the default minority carrier lifetime over the entire pulse length (no lifetime degradation). This curve is labeled $\tau_1 = \tau_2 = 2\text{x}10^{-5}s$, where τ_1 is the minority carrier lifetime before the neutron pulse and τ_2 is the lifetime after the neutron pulse. The convergence to a steady current is evident. The photocurrent density curve directly below the top curve corresponds to the case where $\tau_2 = 2\text{x}10^{-6}s$. It is clear that this photocurrent shows a noticeable decrease when compared with the non-degraded photocurrent over the time spanned after the neutron pulse through the end of the gamma irradiation. The curve corresponding to a degradation of two orders of magnitude, given as $\tau_2 = 2\text{x}10^{-7}s$, shows a more apparent decrease in current (about 40%) to a second steady state associated with this degraded carrier lifetime for the remainder of the gamma pulse. It exhibits a rapid drop to zero during the recovery phase of the gamma pulse. The curves corresponding to $\tau_2 = 2\text{x}10^{-8}s$, and $\tau_2 = 2\text{x}10^{-9}s$ show similar behavior. This example shows a dual steady state behavior resulting from the degraded carrier lifetime.

Figure 4 shows the computation of the analytic photocurrent density in the undepleted n-doped region as a function of time when a neutron pulse follows a gamma irradiation. The solid line indicates the case where there is no pulse or the minority carrier lifetime does not degrade. The dash-dot line indicates the case where the minority carrier lifetime abruptly decreases an order of magnitude due to a neutron pulse at time $t = 0.3\ \mu s$. In this case, we see that over the time period shown that the decrease in photocurrent density compared to the case where there is no lifetime degradation is insignificant. The long dashed line corresponds to a minority carrier lifetime of $\tau_2 = 2\text{x}10^{-7}s$ after the neutron pulse. In this case a very significant decrease in photocurrent occurs and the pulse shape is noticeably affected. The medium dashed line corresponding to the case where $\tau_2 = 2\text{x}10^{-8}s$ shows an even greater drop in photocurrent and the case where $\tau_2 = 2\text{x}10^{-9}s$ drops the photocurrent density to zero within a few nanoseconds.

Figure 5 gives the time history of the excess carrier density associated with Figure 3, for the case where the minority carrier lifetime after the neutron pulse is $\tau_2 = 2\text{x}10^{-7}s$. The z-axis gives the excess carrier density at any point (x, t). The excess carrier density is zero at $x = 0$ and $x = L = 49\mu m$ due to the imposed boundary conditions. From the graph we see that the charge builds up to a steady profile after a few tenths of μs. At $t = 1.5\mu s$, when the minority carrier lifetime abruptly drops due to the neutron pulse, the excess carrier density drops as well. Finally, at the end of the gamma pulse at $t = 2.4\mu s$, the excess carrier density rapidly drops to approach zero.

Figure 6 gives the time history of the excess carrier density associated with Figure 3, for the case where the minority carrier lifetime after the neutron pulse is $\tau_2 = 2\text{x}10^{-8}s$. From the graph we see the same behavior as in Figure 5, but with a significant decrease in excess carrier density after the neutron pulse when compared to the case where $\tau_2 = 2\text{x}10^{-7}s$

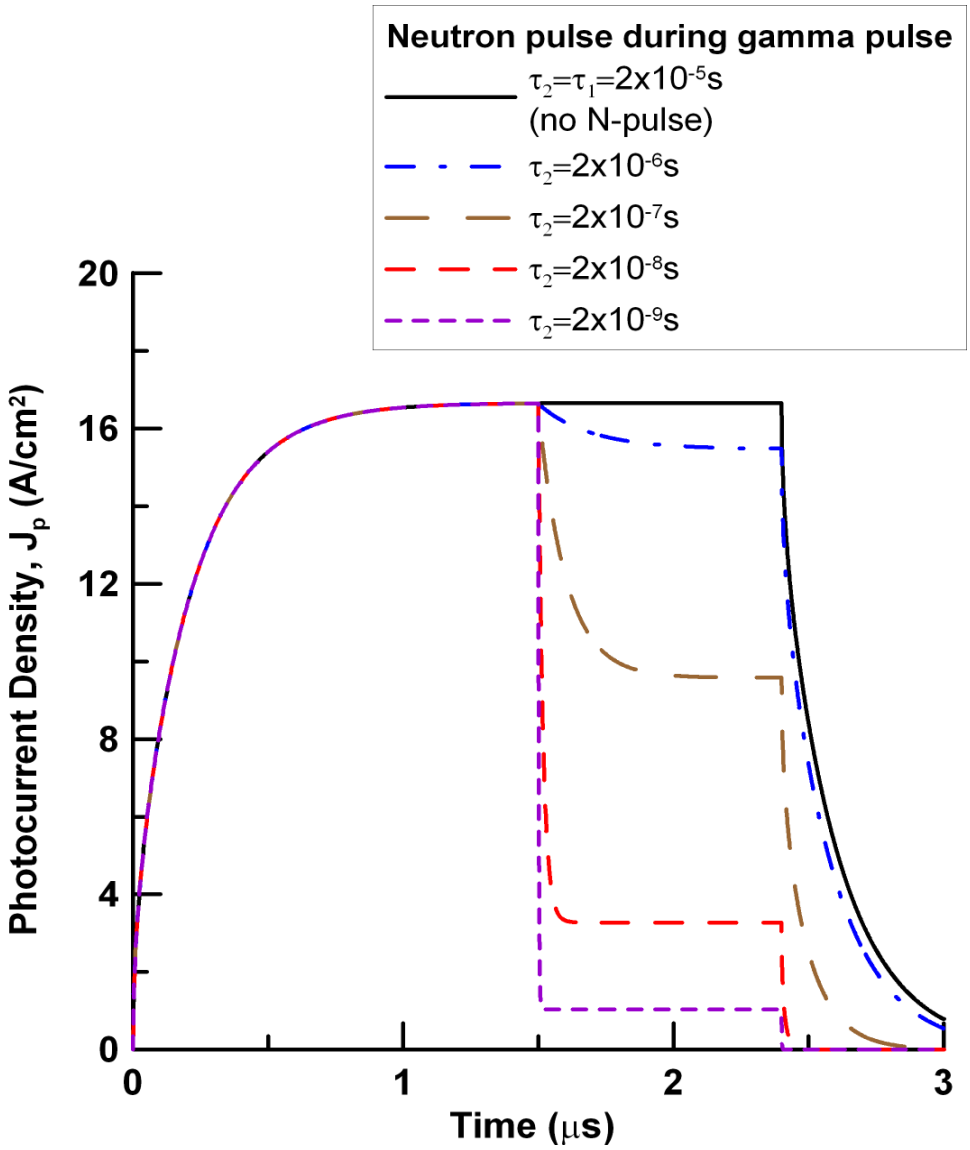

Figure 3: Photocurrent from the undepleted n-doped region of a *pn* diode due to a 2.4μs long, 1x10^9 rad(Si)/s square-wave gamma irradiation with a concurrent neutron pulse at 1.5 μs. τ_1 is the pre-pulse minority carrier lifetime and τ_2 is the post-neutron pulse minority carrier lifetime.

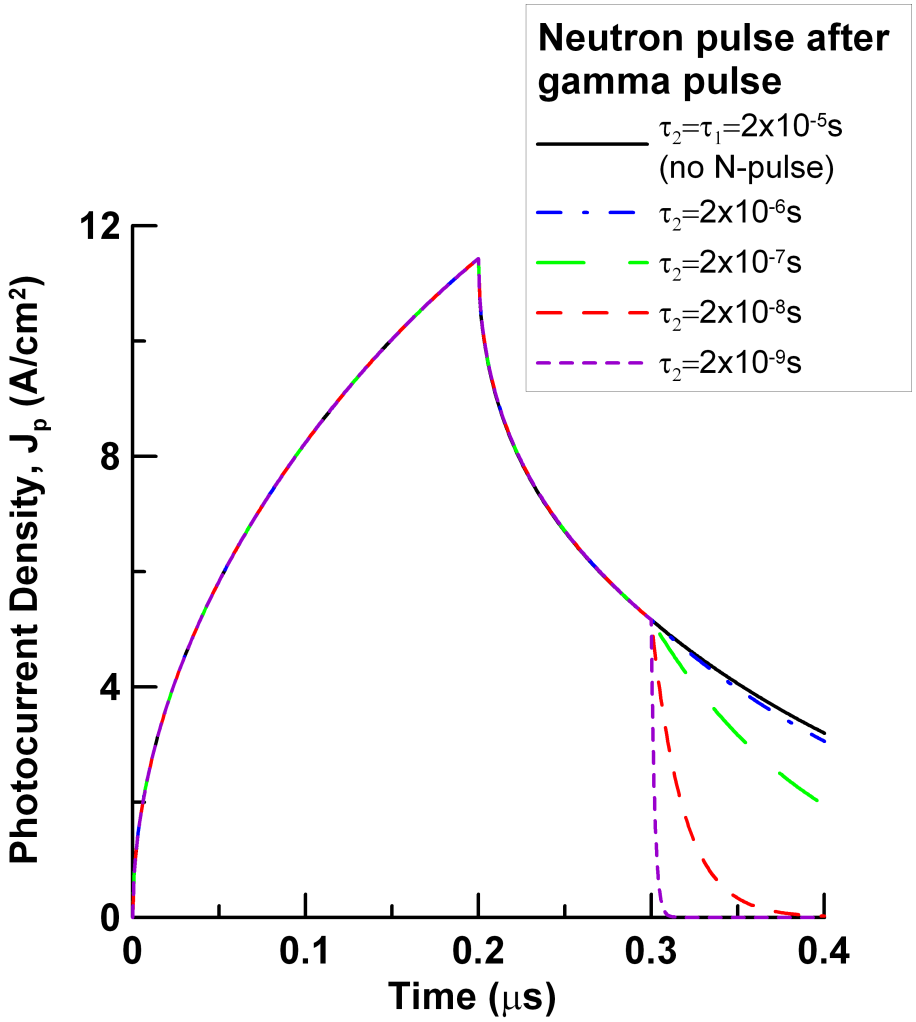

Figure 4: Photocurrent from the undepleted n-doped region of a *pn* diode due to a 0.2 μs long, 1x10^9 rad(Si)/s square-wave gamma irradiation. A neutron pulse occurs after the gamma irradiation at $t = 1.5\mu$s. τ_1 is the pre-neutron pulse minority carrier lifetime and τ_2 is the post-neutron pulse minority carrier lifetime.

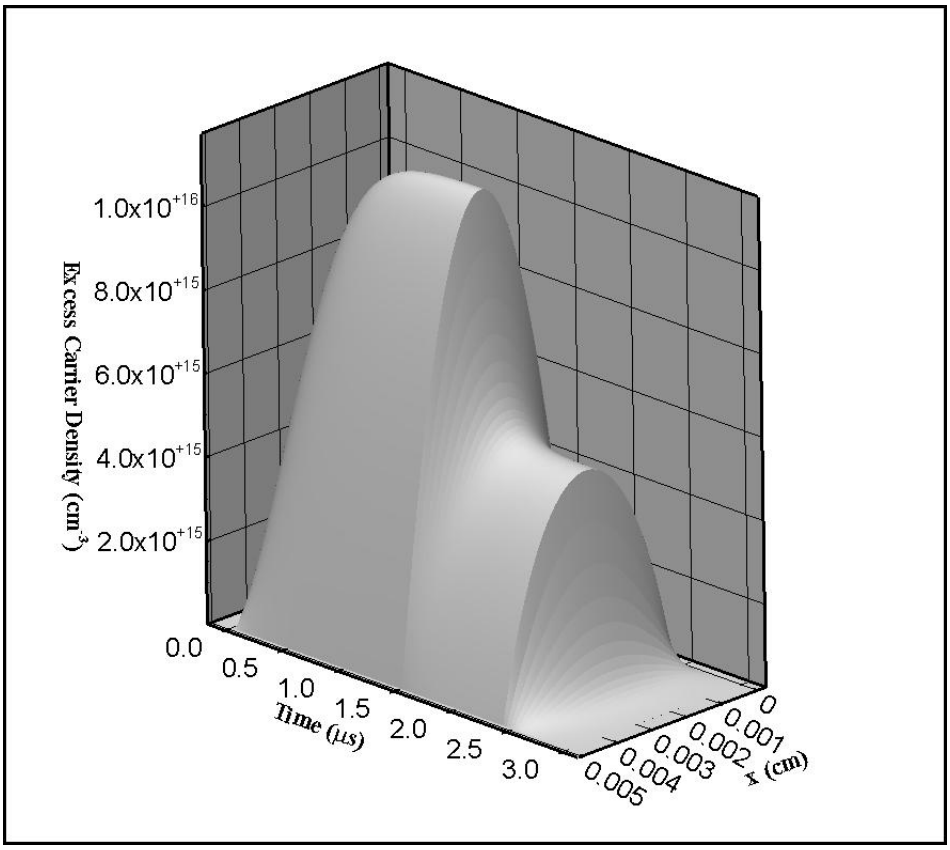

Figure 5: Excess minority carrier density as a function of x and t in the irradiated undepleted n-type region of a pn diode. The diode is gamma-irradiated from $t = 0$ until $t = 2.4\mu s$ and a neutron pulse occurs at $t = 1.5\mu s$. $\tau_1 = 2\text{x}10^{-5}$ is the pre-neutron pulse minority carrier lifetime and $\tau_2 = 2\text{x}10^{-7}$ is the post-neutron pulse minority carrier lifetime. No ohmic field is assumed.

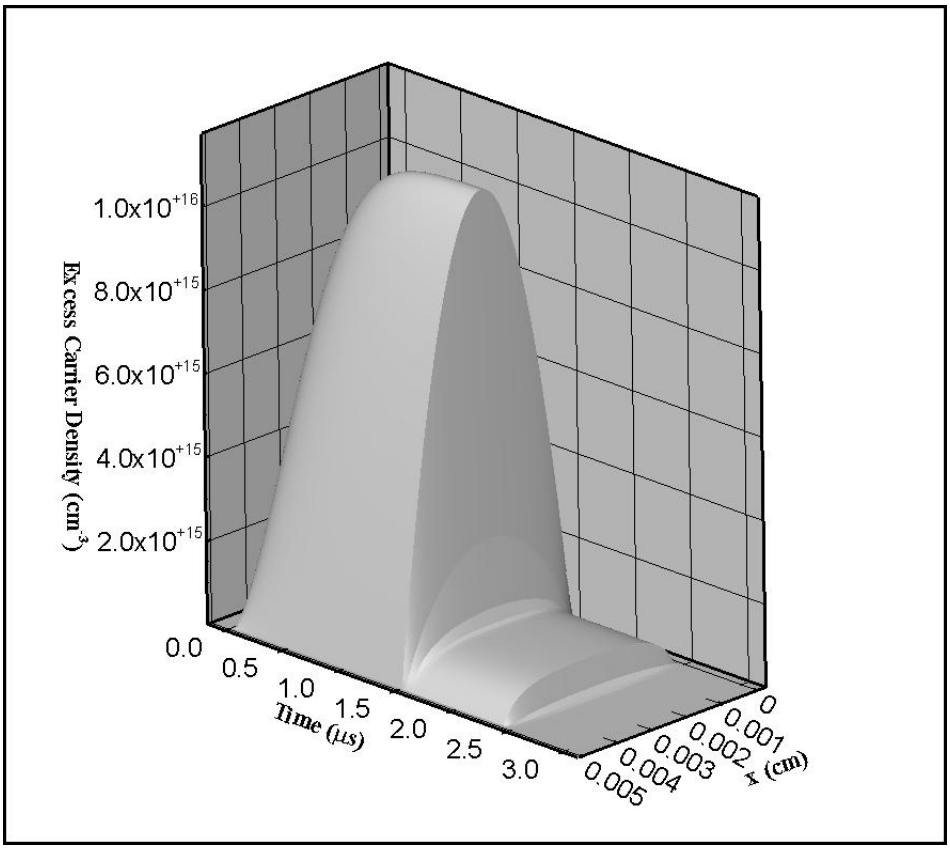

Figure 6: Excess minority carrier density as a function of x and t in the irradiated undepleted n-type region of a pn diode. The diode is gamma-irradiated from $t = 0$ until $t = 2.4\mu s$ and a neutron pulse occurs at $t = 1.5\mu s$. $\tau_1 = 2\text{x}10^{-5}$ is the pre-neutron pulse minority carrier lifetime and $\tau_2 = 2\text{x}10^{-8}$ is the post-neutron pulse minority carrier lifetime. No ohmic field is assumed.

4.2 The lightly doped *pn* diode with an ohmic field

For lightly doped diodes, some of the applied potential invokes a field in the non-depleted regions. The solutions developed in this report allow consideration of a constant ohmic field in the undepleted regions. Figure 7 shows the photocurrent following a gamma irradiation and neutron pulse from the n-type undepleted region of a *pn* diode where an ohmic field of -20 V/cm is assumed. The *pn* diode material parameters used are given in Table 2. The generation function is a $1.0\mu s$ square pulse with $g_0 = 4.3\text{x}10^{22}$ pairs/cm^3-s, corresponding to a radiation pulse of $1\text{x}10^9$ rad(Si)/s.

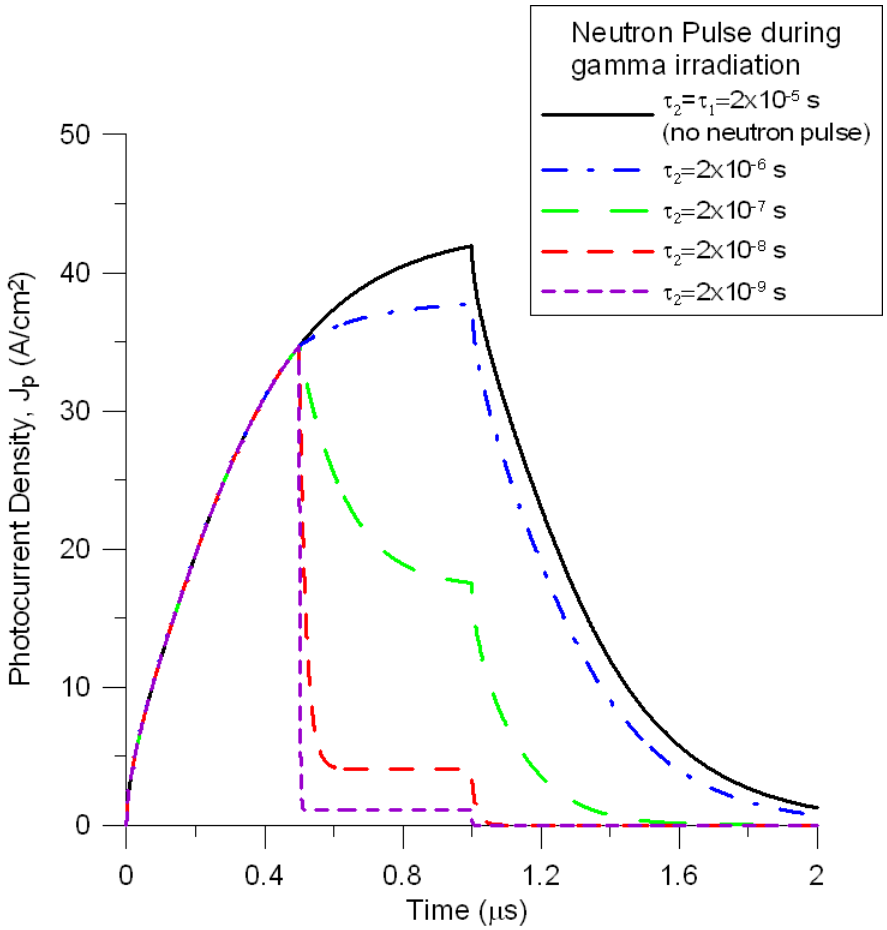

Figure 7: Photocurrent from the undepleted n-doped region of a *pn* diode due to a square-wave gamma irradiation with a concurrent neutron pulse. τ_1 is the pre-pulse minority carrier lifetime and τ_2 is the post-neutron pulse minority carrier lifetime. The effect of an ohmic electric field in the undepleted n-doped region, $E_n = -20$ V/cm is included.

4.3 A lightly doped *pn* diode, J_p with $g(x,t) = g(t)$ piecewise-linear

Our final example shows the minority current from the n-doped region of a *pn* diode, using the equations given in section 3.3. The parameters for this simulation are given in Table 2.

Table 2: Description of parameters used in the lightly doped piecewise-linear *pn* diode simulation.

Parameter	**Description/Units**	**Value for Simulation**
g_i	i_{th} endpoint of $g(t)$ (pairs/cm^3-s) (Fig. 8 only)	$(0, 5, 8, 2, 0)$x10^{22}
t_i	time endpoint of g_i (μs) (Fig. 8 only)	$(0, 1, 2, 4, 5)$
t'	time of neutron irradiation (μs)	0.5, 3.5 (Fig. 8)
E	ohmic field (V/cm)	-20
τ_1	Minority carrier lifetime before neutron pulse (s)	2x10^{-5}
τ_2	Minority carrier lifetime after neutron pulse (s)	2x10^{-7}
μ_p	Minority carrier mobility ($cm^2/(Vs)$)	461
D_p	Minority carrier diffusion coefficient=$\frac{kT\mu_p}{q}$ (cm^2/s)	11.91
L	undepleted n-doped region width (cm)	0.00764
J_p	minority carrier current densities A/cm^2	see figure

Figure 8 gives the photocurrent as a function of time. The solid line with symbols gives the generation density $g(t)$, which is mapped to the right hand axis. The solid line without symbols gives the minority carrier photocurrent density as a function of time for the case where there is no carrier lifetime degradation, while the dashed line gives the minority carrier photocurrent density where there is a two order of magnitude drop in carrier lifetime at t=3.5 μs. The plot shows a significant drop in current due to the loss of carrier lifetime. The generalization of the solution to an arbitrary piecewise linear generation function is useful in finding the photocurrents at experimental facilities where it is difficult to produce a square wave pulse. An example of a more complex generation density and its solution are given in the next section.

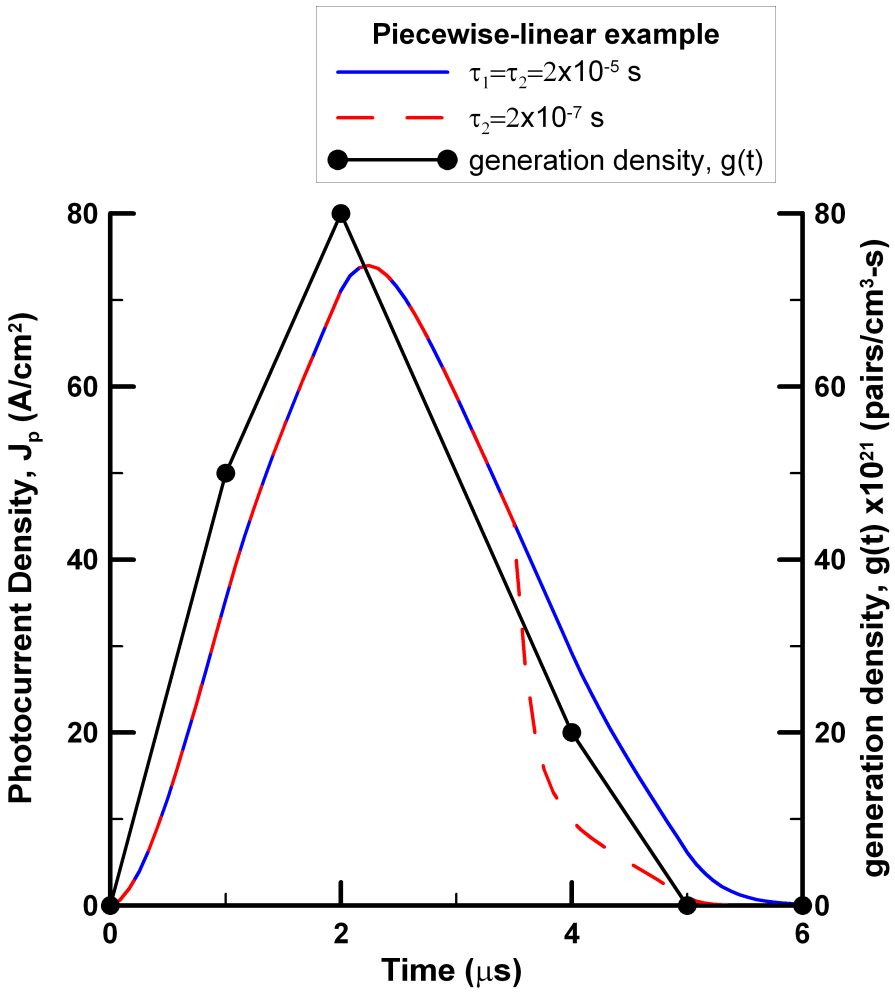

Figure 8: Photocurrent from the undepleted n-doped region of a *pn* diode due to a piecewise-linear gamma irradiation with a neutron pulse at t=3.5 μs. τ_1 is the pre-pulse minority carrier lifetime and τ_2 is the post-neutron pulse minority carrier lifetime. The piecewise linear gamma irradiation generation density is shown by the line with symbols. Other diode parameters are given in Table 2.

5 Convergence and computing time considerations

An important consideration in employing the analytic solutions described in this report is the number of terms necessary to obtain a solution and the accuracy of that solution. This is especially true for equations implemented in circuit codes, because the photocurrents may be computed for hundreds of thousands or millions of devices simultaneously. We will address the accuracy of using the ambipolar diffusion equation approximation to simulate the full set of carrier transport equations in a separate SAND report, where we will compare ADE computed excess carrier and current densities with those obtained through numerical simulation of the full set of equations. Given that the accuracy in using the ADE to simulate radiation or light generated photocurrents is sufficient, it is important to address issues concerning the mathematical convergence of the series presented in this report. We first note that convergence of the raw Fourier sine series, produced by substituting equations (29), (35), or (41) into equations (25) and (26) may be slow for some sets of parameters, requiring a few thousand terms to produce an accurate solution. The slow convergence may be traced to the $\exp(-aL)$ term of equation (18), which becomes very large when $aL = \mu EL/2D$ is large and negative, leading to extreme oscillations in the series. Additionally, the α_n term in the numerator of equation (26) does not help convergence. We will show in this section that the slow convergence of the raw series may be helped significantly by expressing the solution in terms of a closed-form part and a transient part in which exponentially decaying time-dependent terms help convergence. The closed-form part corresponds to steady-state solutions for the step and square-pulse generation densities and to a set of time-dependent line segments for the piecewise linear generation density. The comments of this section are also applicable to the sums given in [9], which have a similar form to those of this report.

Figure 9 gives the minority carrier photocurrent density from the n-type undepleted region of an abrupt *pn* diode with no ohmic field. The photocurrent density is computed from equations (26) and (41) where the equation has been re-indexed as described in section 2.2. For this figure and the rest of the figures in this section, $g(t)$ is defined by the points (t_ix10^{-6} s,g_ix10^{22} pairs/cm^2/s) as $(0,0)$, $(0.5,5)$, $(1,0)$, $(1.5,8)$, $(2,0)$, $(3,5)$, $(5,5)$, and ($\mathrm{t}_M = 7,0$) (see Figure 2). Other parameters are: $t' = 6\mu$s, $\tau_1 = 2$x10^{-5}s, $\tau_2 = 2$x10^{-7}s, $\mu_p = 461$ cm^2/Vs, $D_p = 11.91$ cm^2/s, and $L = 0.00764$ cm. The computations show the effect of the number of terms, n, on the convergence of the raw series when the re-indexed form of equation (41) is used to compute the solution. In this case, we observe that convergence is very rapid, with only a few tens of terms necessary for sufficient accuracy for most calculations.

Figure 10 gives the photocurrent density computed from equations (26) and (41) for a non-zero ohmic electric field with $E_p = -100$ V/cm. In this case, the parameter $aL = -14.7$ and $\exp(-aL) = 2639399$ in equation (18). Figure 10 shows the generation function and the diode current density as a function of time. In this case we see that at least a few thousand terms are necessary for convergence, and that the solution for $n = 100$, where convergence has not been achieved, has a very significant error.

The most effective way to illustrate why the raw series formulas for $J_p(t)$ do not converge particularly well, when e^{-aL} is *large,* is to point out that each of the respective formulas

from Sections 3.1 - 3.3 involve a series which includes a (steady-state) portion of the form:

$$S_{k,1} = \sum_{n=1}^{\infty} \frac{\bar{w}_n \alpha_n}{a_{k,n}} \tag{44}$$

for which, using results from Oberhettinger [20], we were able to show (see Appendix A)

$$S_{k,1} = \sum_{n=1}^{\infty} \frac{\bar{w}_n \alpha_n}{a_{k,n}} = \frac{L\tau_k}{2} \left[-a + \gamma_k \frac{\left(\cosh(\gamma_k L) - e^{-aL}\right)}{\sinh(\gamma_k L)} \right] \tag{45}$$

In practice, however, when we create a computer program to compute $J_p(t)$ (which includes $S_{k,1}$) we must settle for the approximation,

$$S_{k,1}(N) \simeq \sum_{n=1}^{N} \frac{\bar{w}_n \alpha_n}{a_{k,n}} \tag{46}$$

for some finite N.

When $E = 0$ the above equation simplifies (see section 2.2), to become,

$$S_{k,1}(N) \simeq \sum_{n=0}^{N} \frac{2}{a_{k,2n+1}} \tag{47}$$

Using the aforementioned parameters, with $k = 1$ and $E = -100.0$ V/cm, we find that the N in formula (46) must equal 220000 before it agrees (to five significant digits) with the value obtained from the right hand side of equation (45): $S_{1,1} \simeq 2.3582\text{x}10^{-6}$. It was also observed that for the partial sums, $S_{1,1}(999) \simeq 3.0136\text{x}10^{-6}$ and $S_{1,1}(1000) \simeq 1.7030\text{x}10^{-6}$, and the partial sums exhibit this oscillatory type behavior throughout. For the same set of parameters , but with $E = 0$, the re-indexed $S_{1,1}(4835)$ agrees (to five significant digits) with the value obtained from the right hand side of equation (45). We see that when aL is large and negative that the term $\bar{w}_n$ is dominated by the exponential term and oscillates between large positive and negative values. As the index n grows in the series the terms in the denominator will eventually become large and force convergence. The time-dependent exponential terms in $I_n(t)$ do not, however, cause similar convergence concerns because when a is large, so are the parameters $a_{1,n}$ and $a_{2,n}$, producing fairly rapid exponential decay.

As it turns out, the terms not involving time-dependent exponential decay may be be evaluated using the closed form formulas given in Appendix A. Using this methodology, the solutions for the current density are given in sections 3.1 to 3.3. Comparing to the specific

problem shown in Figure 10, Figure 11 shows both the partial closed form minority carrier current density along with the raw series computed with equation (26) using equation (41) with 10,000 terms. We see that convergence using the partial closed form solution, labeled as "partial closed form" in the figure, improves markedly from requiring thousands of terms to only a few tens of terms for accuracy. In particular, using only 20 terms, the current density cannot be differentiated from the plot using 10,000 terms in the raw solution. The 14 term solution is also very close to the 10,000 term raw solution, except near the endpoints of the lines defining $g(t)$ and at the point $t = t'$, where a large error may be seen in the near vertical lines at these points. A larger error occurs at these points because there is less exponential decay from the time dependent part of the series terms near these points.

In the case of the piecewise linear generation function, the closed-form portion of the current density consists of a set of line segments that bound the total current density when the number of terms in the computation is sufficiently large. In the case where a negative ohmic field exists in the undepleted region, the current density approaches the line segments away from the generation function endpoints since the transient time-dependent exponential terms become small in these regions. In the case where there is no ohmic field the current density does not necessarily approach the line segments, but the line segments bound the area in which the current density meanders. The behavior for both of these cases is shown in Figure 12.

Finally, we discuss the improvement in CPU time through implementation of the partial closed form solutions. We note that for the partial closed form solution that only about 20 terms are needed to produce a curve of sufficient accuracy to be indistinguishable from the raw solution computed with 10,000 terms in Figure 11. Figure 10 shows that about 5000 terms are necessary for close agreement with the 10,000 term raw solution. Table 3 gives a comparison of the CPU time required in the FORTRAN programs used to compute these curves on a PC. Each figure consists of 1000 points in time. We note that the FORTRAN programs were not optimized and that these results only serve as an indicator of the relative differences in compute time. It is apparent from Table 3 that at least a couple orders of magnitude improvement in the computational time may be gained by the use of the partial closed form solution. Finally, we note that great improvements in CPU time can likely be made through computation on parallel processors, since the Fourier terms are independent of each other. A copy of the FORTRAN program used in the solution of the partial closed form solution is given in Appendix B.

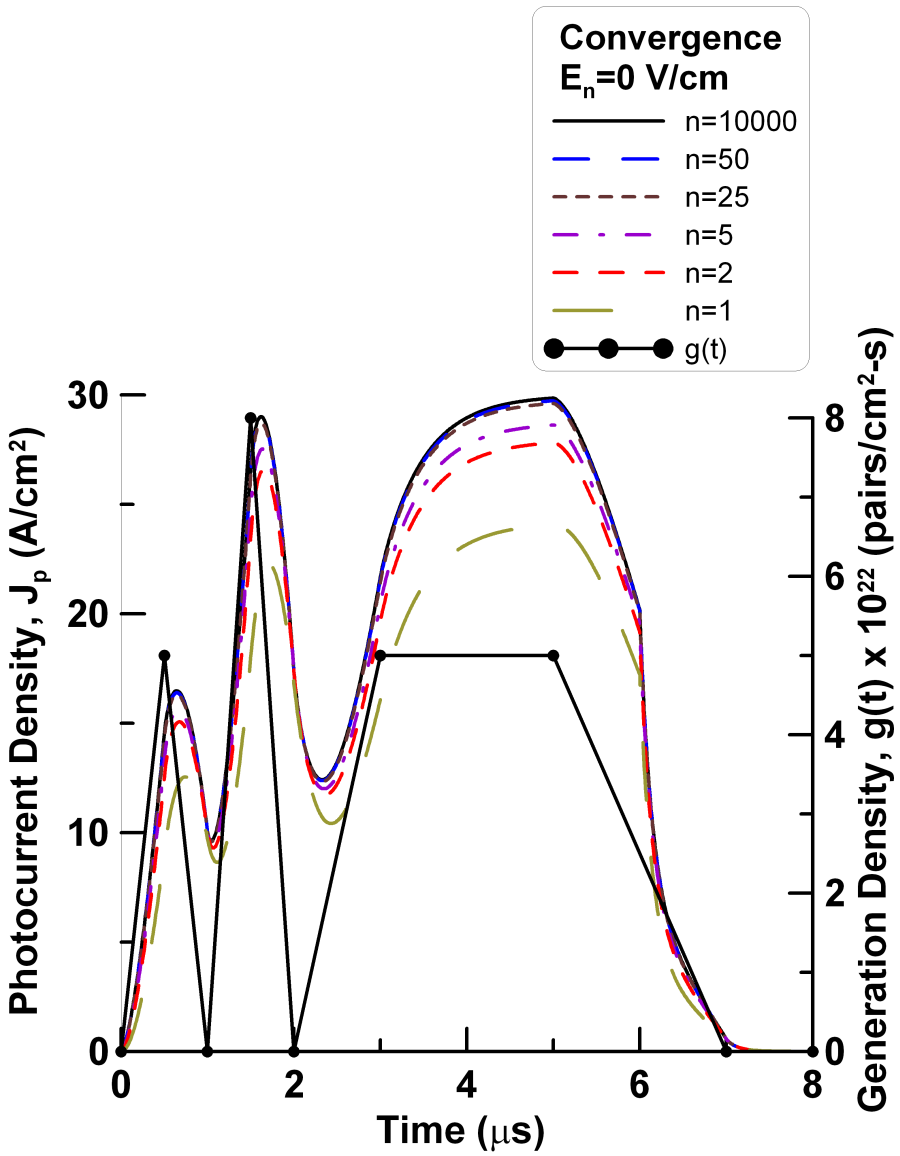

Figure 9: Minority carrier current density convergence from the n-type region of a pn diode as a function of the number or terms, n, used in the raw Fourier sine series, in equations (26) and (41). A zero ohmic field was assumed with a neutron pulse occurring at $t' = 6\mu s$. The solid line with symbols give the generation function, $g(t)$, plotted on the right axis. Other parameters were set as in Table 2.

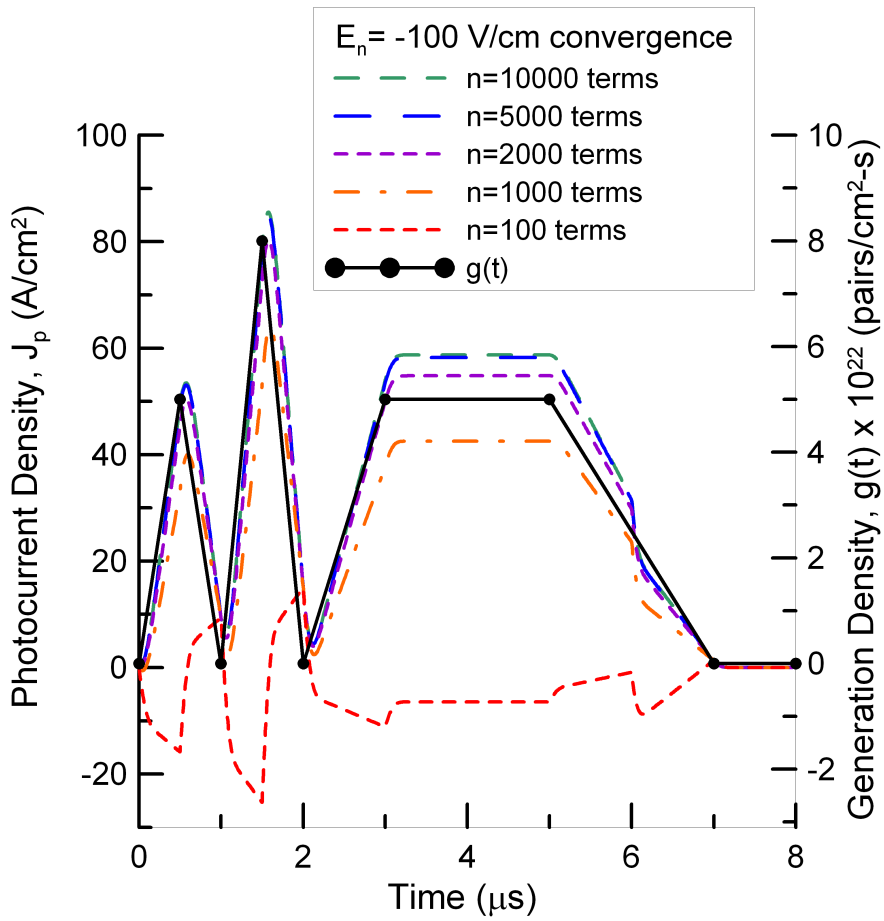

Figure 10: Minority carrier current density convergence from the n-type region of a *pn* diode as a function of the number or terms, n, used in the raw Fourier sine series for the raw solution. A high ohmic field of $E_p = -100$ V/cm was assumed with a neutron pulse occurring at $t' = 6\mu s$. The generation density is shown in the figure. Other parameters were set as in Table 2.

Table 3: Comparison of CPU times for the raw and partial closed form solutions as a function of number of Fourier terms for piecewise-linear *pn* diode simulations. Current density simulations are shown in Figure 11.

Computer code	**number of terms**	**PC CPU times (s)**
raw	2000	0.9680
raw	5000	2.375
raw	10000	4.705
partial closed form	20	0.0156
partial closed form	50	0.0469
partial closed form	2000	0.9375

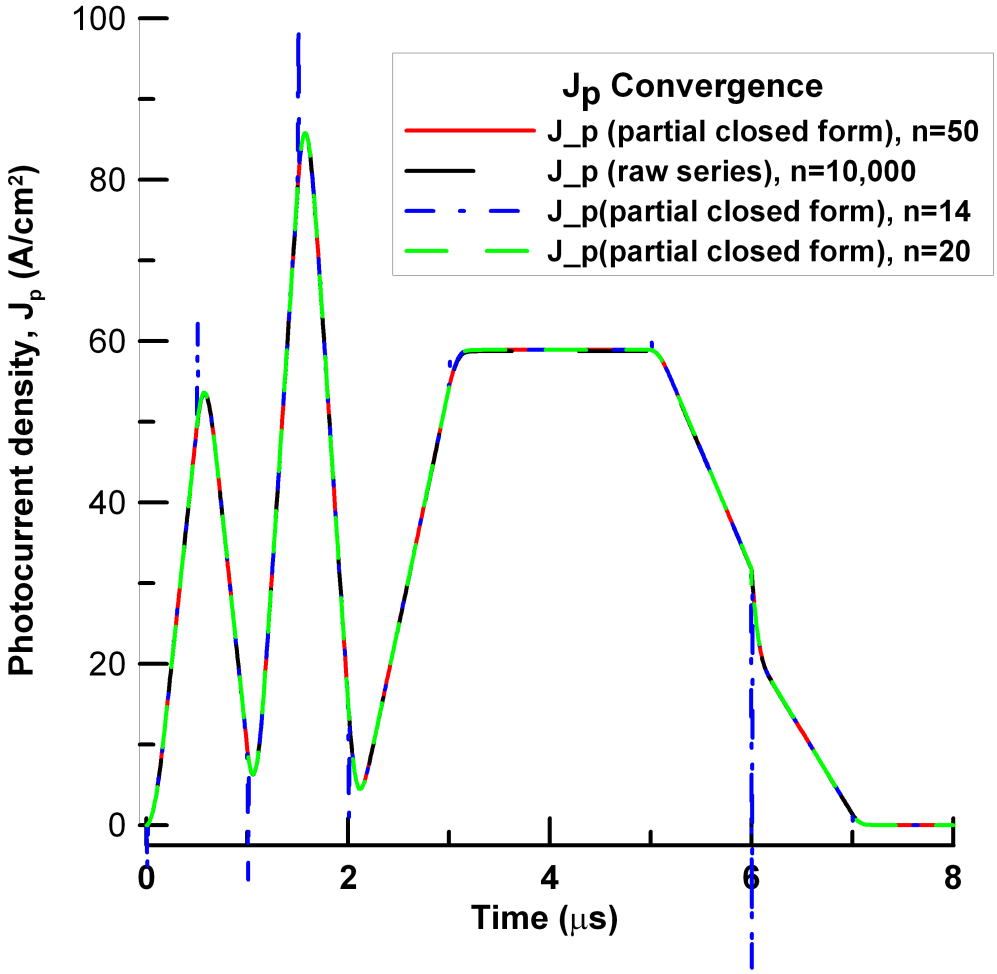

Figure 11: Minority carrier current density convergence from the n-type region of a *pn* diode as a function of the number or terms, n, used in the raw Fourier sine series. This figure shows both the highly convergent solution using closed-form terms (denoted "partial closed form" and given by eq. (43)) and the original solution (denoted "raw", given by eqs. (26) and (41)), before evaluation using the closed form formulas. About 5000 terms are required for convergence of the raw solution while only about 20 are required for the partial closed form solution. A high ohmic field of $E_p = -100$ V/cm was assumed with a neutron pulse occurring at $t' = 6\mu s$. Other parameters were set as in Table 2.

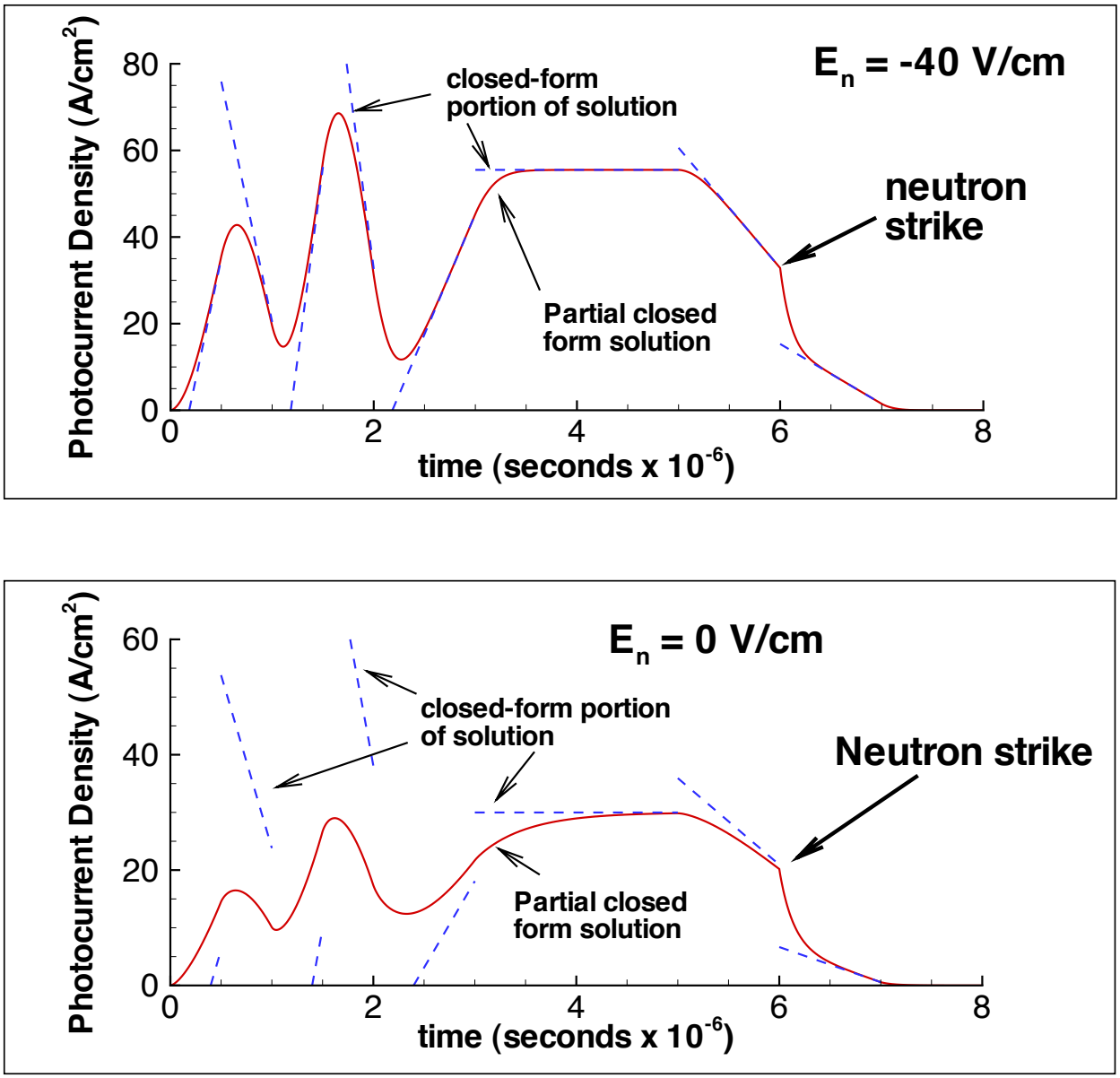

Figure 12: Figure exhibiting minority current density behavior versus time from the undepleted n-doped region of an *np* diode for a negative ohmic field (top) and no ohmic field (bottom). The "closed-form" portions of the solutions are shown by the line segments while the total current densities are given by continuous curves. Note the approach to the closed-form solution as time from the previous generation function endpoint increases. Ohmic fields of $E_p = -40$ V/cm and $E_p = 0$ V/cm were assumed to show the "steady" behavior effectively. Other parameters were set as in Figure 10.

6 Conclusions

In this SAND report we develop new solutions to the 1D ambipolar diffusion equation (ADE), used to approximate the photocurrent produced by a radiation pulse in the undepleted parts of an *np* diode, for the special case in which the minority carrier lifetime is a function of time. Using Fourier sine series techniques developed in [21], we develop a general analytical solution to the 1D ADE for the case where the excess carrier generation (a radiation or light pulse) is a function of time and space, which further simplifies when the excess carrier generation is either a function of time only or of space only. Solutions are developed for the occurrence of a neutron strike, which results in an instantaneous reduction of the carrier lifetimes within the device, either during or after the light or radiation pulse. The carrier lifetime is assumed to be spatially uniform within the device. For the particular case where the gamma pulse is time-dependent only, the solution may be written as an infinite sum with each term consisting of the product of a time-dependent integral and a spatially-dependent sine function. Calculation of the integral may be simplified by using its value at the previous endpoint. A number of cases are explored and illustrated with examples.

For the first case studied, the gamma irradiation is of the form of a step function, $g(x,t) = g_0, t > 0$. In this case, the neutron pulse occurs during the gamma step function irradiation. The carrier lifetimes in each region of the *pn* diode instantaneously decrease at a time $t = t'$ and a reduction of current results that approaches a steady-state current dependent upon the decreased carrier lifetime. Equations are given in subsection 3.1.

For the second case, we assume that the gamma irradiation is of the form of a square pulse, with $g(x,t) = g_0, 0 < t \leq t_1$ and zero for $t > t_1$. The neutron pulse may occur during the gamma irradiation or while the device is recovering from the gamma pulse. The carrier and current densities are given for a sample undepleted n-type region with realistic parameters and a lifetime degradation spanning up to four orders of magnitude for both a highly-doped and a lightly doped diode in section 4. In each case, the current densities are compared to those of a device with no carrier lifetime degradation for neutron strikes occurring both during, and after gamma irradiation. For an order of magnitude degradation of the lifetime only a small reduction in the photocurrent density is observed. For larger reductions in lifetime very significant changes in the photocurrent occur. For long enough pulses, two steady states are observed, one associated with the original carrier lifetime and a second associated with the degraded carrier lifetime. Additionally, we show the time history of the one-dimensional excess carrier density, which shows an abrupt decrease at the time associated with the lifetime degeneration. We also show an example problem where an ohmic field is present, which exhibits an extended current "tail" as compared to the case of no ohmic field. For the case where there is no lifetime degradation the equations are checked and found consistent with those of [9].

Finally, we solve the excess carrier and current densities for the case where $g(x,t) = g(t)$ is piecewise linear with respect to time and the abrupt change in lifetime occurs during or after the pulse. This form of solution is generally incorporated into Xyce or SPICE simulations at SNL and is typically used to characterize the radiation sources at experimental facilities. We

develop a raw solution in which the time-dependent integral for any linear segment of $g(t)$ may be computed in terms of its value at the final point of the previous segment. Although this solution converges, it may require many terms for convergence in the case where an ohmic field is assumed to exist (i.e. lightly doped diodes). The poor convergence may be traced to large non-transient alternating terms in the series. We circumvent this problem by replacing the slower converging components in the raw Fourier series with closed form formulas. Consequently, the only time-dependent terms which remain in the infinite series are of the form $c_n e^{-a_{k,n}T}$ in which $T > 0$, ensuring fast and effective convergence. The newly developed series requires only a few tens of terms for convergence with the accuracy increasing as we move away from the points t' and where the function $g(t)$ changes slope, as T is small close to these points. Examples are given in sections 4 and 5, for the solutions to some fairly complex carrier generation functions for both a zero and large ohmic field.

We attempted to compare our solutions to those produced by numerical device codes such as Medici and Charon. Medici does not currently have a restart ability with the option of changing parameters, so we were unable to make the numerical comparison with this code. The Charon code did not have the capability to do this problem either at the time that we wrote this SAND report. However the source code is maintained in house and personnel offered to modify the code for the comparison. In the end, in the interest of finishing this report in a timely manner, it was decided to forego the numerical comparison to a later SAND report that will look at the validity of the ambipolar transport equation in modeling the advection/transport in semiconductors over a wider range of parameters (dose, doping, etc.).

In recent years the second author of this report has, on occasions, been asked to justify the use of analytic solutions to photocurrent problems, especially when device codes capable of considering complex geometries and non-linear effects are available. In addition to the reasons offered at the beginning of this report, we note that in some cases it may be much faster to develop an analytic solution and a small FORTRAN program than to modify a large code, even if the code source is available, which is not generally the case for commercial codes. Analytic solutions also give an independent verification of a numerical solution. They may also be used to quantify the importance of an effect, and may indicate combinations of parameters that have a physical meaning, such as the parameters $a_{1,n}$ and $a_{2,n}$ in this analysis. Finally, we note that the photocurrent solutions of this paper as well as all of the past papers in the reference section use mathematical tools that were developed in the late 1960s and early 1970s or earlier. Thus, all of this work could have been completed in that time period with the proper mathematical focus by a research organization.

References

[1] L. W. Nagel, SPICE2: A Computer Program to Simulate Semiconductor Circuits, ERL Memo No. ERL-M5250, Electronics Research Laboratory, University of California, Berkeley, May 1975.

[2] Medici User Guide, Ver.Y-2006.06, Synopsis, Mountain View, CA, June 2006.

[3] M. S. Mock, Proc. of NASECODE III Conference, Dublin, Ireland, 1911 (1983).

[4] PADRE 2.3E Reference Manual, AT&T Bell Labs, Murray Hill, NJ, 1993. (also http://nanohub.org/resources/padre/usage)

[5] H. K. Thornquist, E. R. Keiter, R. J. Hoekstra, D. M. Day, and E. G. Boman, A parallel preconditioning strategy for efficient transistor-level circuit simulation, *Computer-Aided Design - Digest of Technical Papers, ICCAD 2009, IEEE/ACM International Conference on Computer-Aided Design*, San Jose, CA, Nov. 2-5, 2009.

[6] J. P. McKelvey, *Solid State and Semiconductor Physics*, Robert E. Krieger Publishing Company, Malabar, Florida, 1966.

[7] W. van Roosbroeck, *Phys. Rev.*, **91**, 282 (1953).

[8] J. L. Wirth and S. C. Rogers, The Transient Response of Transistors and Diodes to Ionizing Radiation, IEEE Trans. Nuc. Sci., **NS-11**, p.24-38 (1964).

[9] C. L. Axness, B. Kerr, and T. F. Wunsch, Analytic light- or radiation-induced *pn* junction photocurrent solutions to the multidimensional ambipolar diffusion equation, *J. Appl. Phys.*, Vol. 96, No. 5, 1 Sept. 2004.

[10] D. M. Long, J R. Florian and R. H. Casey, Transient Response Model for Epitaxial Transistors, IEEE Trans. Nuc. Sci., **NS-30**(6), p.4131-4134 (1983).

[11] O. M. Stuetzer, Extended Steady-State Analysis of the Gamma-Irradiated Cartesian P-N Junction, SAND86-7174, Sandia National Laboratories, Albuquerque, NM (1987).

[12] E. W. Enlow and D. R. Alexander, Photocurrent Modeling of Modern Microcircuit PN Junctions, IEEE Trans. Nuc. Sci., **NS-35** (6), p.1467-1474 (1988).

[13] T. F. Wunsch and C. L. Axness, Modeling the Time-Dependent Transient Radiation Response of Semiconductor Junctions, IEEE Trans. Nuc. Sci., **NS-39** (6), (1992).

[14] J. R. Srour, S. C. Chen, S. Othmer, and R. A. Hartman, Neutron damage mechanisms in charge transfer devices, *IEEE Trans. Nucl. Sci.,* **NS-25**, **6**, pp. 1251-1260, (1978).

[15] J. R. Srour, C. J. Marshall, and P. W. Marshall, A review of displacement damage effects in silicon devices, *IEEE Trans. Nucl. Sci.,* Vol. 50, **3**, pp. 653-670, (2003).

[16] O. L. Curtis, Jr., R. F. Bass, and C. A. Germano, Impurity effects in neutron-irradiated silicon and germanium, Notronics Newbury Park Applied Research Dept., 1965.

[17] C. H. Seager, R. M. Fleming, D. V. Lang, P. J. Cooper, E. Bielejec, and J. M. Campbell, Effects of defect clustering in neutron irradiated silicon, Physica B: Condensed Matter, Volumes 401-402, Dec. 15, 2007, pp 491-494 2007.

[18] G. C. Messenger, A two level model for lifetime reduction process in neutron irradiated silicon and germanium, *IEEE Trans. Nucl. Sci.,* **NS-14**, Dec. 1967.

[19] G. C. Messenger and M. S. Ash, *The effects of Radiation on Electronic Systems*, Van Nostand Reinhold, New York, 1992.

[20] F. Oberhettinger, *Fourier Expansions*, Academic Press, NY, 1973.

[21] M. N. Özişik, *Boundary Value Problems of Heat Conduction*, International Textbook, Scranton, PA, 1968.

Appendix A: Closed-form and steady state analysis

In this appendix we develop the analytic solutions for the excess carrier and current densities as partial closed form solutions. That is, we replace, where possible, any infinite sums contained within the solutions given in section 3 by closed-form formulas. In the case where $g(t)$ is a step or square function, the closed-form evaluations become steady-state solutions in the sense that they are approached as time increases. In the case where $g(t)$ is represented as a piecewise-linear function, the closed-form part of the solution is a piecewise-linear function of time. The four required sums may be derived as follows. Consider,

$$S(x)_{k,1} = \sum_{n=1}^{\infty} \frac{\bar{w}_n \sin(\alpha_n x)}{a_{k,n}} = \sum_{n=1}^{\infty} \frac{\alpha_n (1-(-1)^n e^{-aL})}{(\alpha_n^2 + a^2)\left(D\,(\alpha_n^2 + a^2) + \frac{1}{\tau_k}\right)} \sin(\alpha_n x) \tag{A-1}$$

Applying the relevant partial fraction decomposition to the right hand side produces a pair of like series. Both series may then be replaced by the Fourier expansion formula (see pg. 13, Oberhettinger [20]),

$$\sum_{n=1}^{\infty} (1-(-1)^n C) \frac{n}{(\alpha_n^2 + b^2)} \sin(\alpha_n x) = \frac{L^2}{2\pi} \left[\frac{\sinh(b(L-x))}{\sinh(Lb)} + C \frac{\sinh(bx)}{\sinh(Lb)} \right], 0 < x < L \tag{A-2}$$

Hence

$$S(x)_{k,1} = \frac{L\tau_k}{2} \left[e^{-ax} - \frac{\sinh(\gamma_k(L-x)) + e^{-aL}\sinh(\gamma_k x)}{\sinh(\gamma_k L)} \right],\ 0 \le x \le L \tag{A-3}$$

in which $\gamma_k^2 = a^2 + \frac{1}{D\tau_k}$.

Differentiating equation A-3 with respect to x , then replacing each x with zero, reveals that

$$S_{k,1} = \sum_{n=1}^{\infty} \frac{\bar{w}_n \alpha_n}{a_{k,n}} = \frac{L\tau_k}{2} \left[-a + \gamma_k \frac{\left(\cosh(\gamma_k L) - e^{-aL}\right)}{\sinh(\gamma_k L)} \right] \tag{A-4}$$

Then, respectively differentiating both sides of equations (A-3) and (A-4), with respect to

τ_k , we find that

$$
\begin{aligned}
S(x)_{k,2} &= \sum_{n=1}^{\infty} \frac{\bar{w}_n \sin(\alpha_n x)}{(a_{k,n})^2} \\
&= \frac{L\tau_k^2}{2}\left[e^{-ax} - \frac{\big(\sinh(\gamma_k(L-x)) + e^{-aL}\sinh(\gamma_k x)\big)}{\sinh(\gamma_k L)}\right] + \\
&\quad \frac{L\tau_k}{4D\gamma_k \sinh^2(\gamma_k L)} \cdot \Big[L\sinh(\gamma_k x) - x\sinh(\gamma_k L)\cosh(\gamma_k(L-x)) \\
&\quad + e^{-aL}(x\sinh(\gamma_k L)\cosh(\gamma_k x) - L\sinh(\gamma_k x)\cosh(\gamma_k L))\Big],\ 0 \le x \le L \qquad \text{(A-5)}
\end{aligned}
$$

and

$$
\begin{aligned}
S_{k,2} &= \sum_{n=1}^{\infty} \frac{\bar{w}_n \alpha_n}{(a_{k,n})^2} = \frac{L\tau_k^2}{2}\left[-a + \gamma_k \frac{\big(\cosh(\gamma_k L) - e^{-aL}\big)}{\sinh(\gamma_k L)}\right] \\
&\quad - \frac{L\tau_k\big(\sinh(\gamma_k L)\cosh(\gamma_k L) - e^{-aL}\sinh(\gamma_k L) - \gamma_k L + \gamma_k L\cosh(\gamma_k L)e^{-aL}\big)}{4D\gamma_k \sinh^2(\gamma_k L)} \qquad \text{(A-6)}
\end{aligned}
$$

Formulas (A-4) and (A-6) are required for computing $J_p(t)$ while (A-3) and (A-5) are required for computing $u(x,t)$. Formulas (A-5) and (A-6) are only required for the case of a piecewise continuous linear $g(t)$.

Closed-form and steady state analysis for g(t) a step function

We proceed with the derivation of the partial closed form solutions for the step function of section 3.1. From equations (25), (26), and (29), for $0 < t \le t'$,

$$
\begin{aligned}
u(x,t) &= \frac{2g_0 e^{ax}}{L}\sum_{n=1}^{\infty} \bar{w}_n \frac{1 - e^{-a_{1,n}t}}{a_{1,n}} \sin(\alpha_n x) \\
&= \frac{2g_0 e^{ax}}{L}\sum_{n=1}^{\infty} \frac{\bar{w}_n}{a_{1,n}} \sin(\alpha_n x) - \frac{2g_0 e^{ax}}{L}\sum_{n=1}^{\infty} \bar{w}_n \frac{e^{-a_{1,n}t}}{a_{1,n}} \sin(\alpha_n x) \qquad \text{(A-7)}
\end{aligned}
$$

Thus from equation (A-3),

$$
\begin{aligned}
u(x,t) &= g_0\tau_1\left[1 - e^{ax}\frac{\big(\sinh(\gamma_1(L-x)) + e^{-aL}\sinh(\gamma_1 x)\big)}{\sinh(\gamma_1 L)}\right] \\
&\quad -\frac{2g_0e^{ax}}{L}\sum_{n=1}^{\infty}\bar{w}_n\frac{e^{-a_{1,n}t}}{a_{1,n}}\sin(\alpha_n x)
\end{aligned} \tag{A-8}
$$

and for $t' < t$

$$
\begin{aligned}
u(x,t) &= \frac{2g_0e^{ax}}{L}\sum_{n=1}^{\infty}\bar{w}_n\left[\frac{1-e^{-a_{1,n}t'}}{a_{1,n}}e^{-a_{2,n}(t-t')} + \frac{1-e^{-a_{2,n}(t-t')}}{a_{2,n}}\right]\sin(\alpha_n x) \\
&= \frac{2g_0e^{ax}}{L}\sum_{n=1}^{\infty}\frac{\bar{w}_n}{a_{2,n}}\sin(\alpha_n x) + \frac{2g_0e^{ax}}{L}\sum_{n=1}^{\infty}\bar{w}_n\cdot \\
&\quad \left[\frac{1-e^{-a_{1,n}t'}}{a_{1,n}}e^{-a_{2,n}(t-t')} - \frac{e^{-a_{2,n}(t-t')}}{a_{2,n}}\right]\sin(\alpha_n x)
\end{aligned} \tag{A-9}
$$

or

$$
\begin{aligned}
u(x,t) &= g_0\tau_2\left[1 - e^{ax}\frac{\big(\sinh(\gamma_2(L-x)) + e^{-aL}\sinh(\gamma_2 x)\big)}{\sinh(\gamma_2 L)}\right] + \\
&\quad \frac{2g_0e^{ax}}{L}\sum_{n=1}^{\infty}\bar{w}_n\left[\frac{1-e^{-a_{1,n}t'}}{a_{1,n}}e^{-a_{2,n}(t-t')} - \frac{e^{-a_{2,n}(t-t')}}{a_{2,n}}\right]\sin(\alpha_n x)
\end{aligned} \tag{A-10}
$$

Thus,

$$
u(x,t) = \begin{cases} u_{s,1}(x) - \frac{2g_0e^{ax}}{L}\sum_{n=1}^{\infty}\bar{w}_n\frac{e^{-a_{1,n}t}}{a_{1,n}}\sin(\alpha_n x) & , \quad 0 < t \le t' \\ u_{s,2}(x) + \frac{2g_0e^{ax}}{L}\sum_{n=1}^{\infty}\bar{w}_n\left[\frac{1-e^{-a_{1,n}t'}}{a_{1,n}}e^{-a_{2,n}(t-t')} - \frac{e^{-a_{2,n}(t-t')}}{a_{2,n}}\right]\sin(\alpha_n x) & , \quad t' < t \end{cases} \tag{A-11}
$$

where,

$$u_{s,k}(x) = g_0\tau_k \left[1 - e^{ax}\frac{\big(\sinh(\gamma_k(L-x)) + e^{-aL}\sinh(\gamma_k x)\big)}{\sinh(\gamma_k L)}\right]$$

We proceed next with the derivation of the partial closed form solutions of equation (26). From equation (26) using equation (29), for $0 < t \leq t'$,

$$J_p(t) = \frac{2qDg_0}{L}\sum_{n=1}^{\infty}\bar{w}_n\alpha_n\frac{1-e^{-a_{1,n}t}}{a_{1,n}} = \frac{2qDg_0}{L}\sum_{n=1}^{\infty}\frac{\bar{w}_n\alpha_n}{a_{1,n}} - \frac{2qDg_0}{L}\sum_{n=1}^{\infty}\bar{w}_n\alpha_n\frac{e^{-a_{1,n}t}}{a_{1,n}} \tag{A-12}$$

Therefore,

$$J_p(t) = qDg_0\tau_1\left[-a + \gamma_1\frac{\big(\cosh(\gamma_1 L) - e^{-aL}\big)}{\sinh(\gamma_1 L)}\right] - \frac{2qDg_0}{L}\sum_{n=1}^{\infty}\bar{w}_n\alpha_n\frac{e^{-a_{1,n}t}}{a_{1,n}} \tag{A-13}$$

and similarly , for $t' < t$

$$\begin{aligned} J_p(t) \;=\; & qDg_0\tau_2\left[-a + \gamma_2\frac{\big(\cosh(\gamma_2 L) - e^{-aL}\big)}{\sinh(\gamma_2 L)}\right] + \\ & \frac{2qDg_0}{L}\sum_{n=1}^{\infty}\bar{w}_n\alpha_n\left[\frac{1-e^{-a_{1,n}t'}}{a_{1,n}}e^{-a_{2,n}(t-t')} - \frac{e^{-a_{2,n}(t-t')}}{a_{2,n}}\right] \end{aligned} \tag{A-14}$$

so, in summary,

$$J_p(t) = \begin{cases} J_{s,1} - \frac{2qDg_0}{L}\sum_{n=1}^{\infty}\bar{w}_n\alpha_n\frac{e^{-a_{1,n}t}}{a_{1,n}} & , \quad 0 < t \leq t' \\ J_{s,2} + \frac{2qDg_0}{L}\sum_{n=1}^{\infty}\bar{w}_n\alpha_n\left[\frac{1-e^{-a_{1,n}t'}}{a_{1,n}}e^{-a_{2,n}(t-t')} - \frac{e^{-a_{2,n}(t-t')}}{a_{2,n}}\right] & , \quad t' < t \end{cases} \tag{A-15}$$

in which

$$J_{s,k} = qDg_0\tau_k\left[-a + \gamma_k\frac{\big(\cosh(\gamma_k L) - e^{-aL}\big)}{\sinh(\gamma_k L)}\right] \tag{A-16}$$

Closed-form and steady state analysis for g(t) a square pulse

We proceed next with the derivation of the partial closed form solutions for the square pulse function of section 3.2. Noting that the first two components of formula (35) are identical to the two components of $I_n(t)$ in equation (29), it follows for $t' \leq t_1$ that,

$$u(x,t) = \begin{cases} u_{s,1}(x) - \frac{2g_0 e^{ax}}{L} \sum_{n=1}^{\infty} \bar{w}_n \frac{e^{-a_{1,n}t}}{a_{1,n}} \sin(\alpha_n x) & , \quad 0 < t \leq t' \\ u_{s,2}(x) + \frac{2g_0 e^{ax}}{L} \sum_{n=1}^{\infty} \bar{w}_n \left[\frac{1-e^{-a_{1,n}t'}}{a_{1,n}} e^{-a_{2,n}(t-t')} - \frac{e^{-a_{2,n}(t-t')}}{a_{2,n}} \right] \sin(\alpha_n x) & , \quad t' < t \leq t_1 \end{cases} \tag{A-17}$$

and for $t > t_1$

$$u(x,t) = \frac{2g_0 e^{ax}}{L} \sum_{n=1}^{\infty} \bar{w}_n \left[\frac{1-e^{-a_{1,n}t'}}{a_{1,n}} e^{-a_{2,n}(t-t')} + \frac{1-e^{-a_{2,n}(t_1-t')}}{a_{2,n}} e^{-a_{2,n}(t-t_1)} \right] \sin(\alpha_n x) \tag{A-18}$$

Therefore,

$$u(x,t) = \begin{cases} u_{s,1}(x) - \frac{2g_0 e^{ax}}{L} \sum_{n=1}^{\infty} \bar{w}_n \frac{e^{-a_{1,n}t}}{a_{1,n}} \sin(\alpha_n x) & 0 < t \leq t' \\ u_{s,2}(x) + \frac{2g_0 e^{ax}}{L} \sum_{n=1}^{\infty} \bar{w}_n \left[\frac{1-e^{-a_{1,n}t'}}{a_{1,n}} e^{-a_{2,n}(t-t')} - \frac{e^{-a_{2,n}(t-t')}}{a_{2,n}} \right] \sin(\alpha_n x) & t' < t \leq t_1 \\ \frac{2g_0 e^{ax}}{L} \sum_{n=1}^{\infty} \bar{w}_n \left[\frac{1-e^{-a_{1,n}t'}}{a_{1,n}} e^{-a_{2,n}(t-t')} + \frac{1-e^{-a_{2,n}(t_1-t')}}{a_{2,n}} e^{-a_{2,n}(t-t_1)} \right] \sin(\alpha_n x) & t > t_1 \end{cases} \tag{A-19}$$

Utilizing the above equation directly in equation (5), we may evaluate $J_p(t)$ as

$$J_p(t) = \begin{cases} J_{s,1} - \frac{2qDg_0}{L}\sum_{n=1}^{\infty}\bar{w}_n\alpha_n\frac{e^{-a_{1,n}t}}{a_{1,n}} & 0 < t \leq t' \\ J_{s,2} + \frac{2qDg_0}{L}\sum_{n=1}^{\infty}\bar{w}_n\alpha_n\left[\frac{1-e^{-a_{1,n}t'}}{a_{1,n}}e^{-a_{2,n}(t-t')} - \frac{e^{-a_{2,n}(t-t')}}{a_{2,n}}\right] & t' < t \leq t_1 \\ \frac{2qDg_0}{L}\sum_{n=1}^{\infty}\bar{w}_n\alpha_n\left[\frac{1-e^{-a_{1,n}t'}}{a_{1,n}}e^{-a_{2,n}(t-t')} + \frac{1-e^{-a_{2,n}(t_1-t')}}{a_{2,n}}e^{-a_{2,n}(t-t_1)}\right] & t > t_1 \end{cases} \tag{A-20}$$

where $J_{s,k}$ are given by equation (33).

In the case where $t' > t_1$, from equation (36),

$$u(x,t) = \begin{cases} u_{s,1}(x) - \frac{2g_0e^{ax}}{L}\sum_{n=1}^{\infty}\bar{w}_n\frac{e^{-a_{1,n}t}}{a_{1,n}}\sin(\alpha_n x) & 0 < t \leq t_1 \\ \frac{2g_0e^{ax}}{L}\sum_{n=1}^{\infty}\bar{w}_n e^{-a_{1,n}(t-t_1)}\frac{\left(1-e^{-a_{1,n}t_1}\right)}{a_{1,n}}\sin(\alpha_n x) & t_1 < t \leq t' \\ \frac{2g_0e^{ax}}{L}\sum_{n=1}^{\infty}\bar{w}_n e^{-a_{2,n}(t-t')}e^{-a_{1,n}(t'-t_1)}\frac{\left(1-e^{-a_{1,n}t_1}\right)}{a_{1,n}}\sin(\alpha_n x) & t > t' \end{cases} \tag{A-21}$$

and

$$J_p(t) = \begin{cases} J_{s,1} - \frac{2qDg_0}{L}\sum_{n=1}^{\infty}\bar{w}_n\alpha_n\frac{e^{-a_{1,n}t}}{a_{1,n}} & 0 < t \leq t_1 \\ \frac{2qDg_0}{L}\sum_{n=1}^{\infty}\bar{w}_n\alpha_n e^{-a_{1,n}(t-t_1)}\frac{\left(1-e^{-a_{1,n}t_1}\right)}{a_{1,n}} & t_1 < t \leq t' \\ \frac{2qDg_0}{L}\sum_{n=1}^{\infty}\bar{w}_n\alpha_n e^{-a_{2,n}(t-t')}e^{-a_{1,n}(t'-t_1)}\frac{\left(1-e^{-a_{1,n}t_1}\right)}{a_{1,n}} & t > t' \end{cases} \tag{A-22}$$

Closed-form and steady state analysis for g(t) piecewise-linear

Now in Section 3.3 our formula for $I_n(t)$ is comprised of four separate portions. Within these respective portions are the following terms, which cause equation (41) to converge less

efficiently.

$$I_{n,cf}(t) = \begin{cases} \frac{h_m(t-t_m)+g_m-\frac{h_m}{a_{1,n}}}{a_{1,n}} & , \quad 0 < t \leq t' \\ \\ \frac{h_m(t-t_m)+g_m-\frac{h_m}{a_{2,n}}}{a_{2,n}} & , \quad t_m \leq t' < t \\ \\ \frac{h_s(t-t_s)+g_s-\frac{h_s}{a_{2,n}}}{a_{2,n}} & , \quad t_s < t \end{cases} \tag{A-23}$$

Utilizing equations (A-3) and (A-5), the partial closed form of the series for $u(x,t)$ may be written,

$$u(x,t) = \frac{2e^{ax}}{L} \cdot \begin{cases} [h_m(t-t_m)+g_m]\, S(x)_{1,1} \\ -h_m S(x)_{1,2} + \sum\limits_{n=1}^{\infty} \bar{w}_n R_n(t) \sin(\alpha_n x), & 0 \leq t_m < t \leq t' < t_{m+1} \\ \\ [h_m(t-t_m)+g_m]\, S(x)_{2,1} \\ -h_m S(x)_{2,2} + \sum\limits_{n=1}^{\infty} \bar{w}_n R_n(t) \sin(\alpha_n x), & t_m \leq t' < t \leq t_{m+1} \\ \\ [h_s(t-t_s)+g_s]\, S(x)_{2,1} \\ -h_s S(x)_{2,2} + \sum\limits_{n=1}^{\infty} \bar{w}_n R_n(t) \sin(\alpha_n x), & t_{m+1} < t_s < t \leq t_{s+1} \leq t_M \\ \\ \sum\limits_{n=1}^{\infty} \bar{w}_n R_n(t) \sin(\alpha_n x), & t > t_M \end{cases} \tag{A-24}$$

where on the four respective intervals

$$R_n(t) =$$

$$\begin{cases} \frac{1}{a_{1,n}} \left\{ \sum_{i=0}^{m-1} \left[\left(g_{i+1} - \frac{h_i}{a_{1,n}} \right) e^{-a_{1,n}(t-t_{i+1})} - \left(g_i - \frac{h_i}{a_{1,n}} \right) e^{-a_{1,n}(t-t_i)} \right] \right. \\ \left. - \left(g_m - \frac{h_m}{a_{1,n}} \right) e^{-a_{1,n}(t-t_m)} \right\}, & 0 \le t_m < t \le t' < t_{m+1} \\ \\ I_n(t') e^{-a_{2,n}(t-t')} - \frac{1}{a_{2,n}} \left\{ \left(h_m (t' - t_m) + g_m - \frac{h_m}{a_{2,n}} \right) e^{-a_{2,n}(t-t')} \right\} & t_m \le t' < t \le t_{m+1} \\ \\ I_n(t_{m+1}) e^{-a_{2,n}(t-t_{m+1})} + \\ \frac{1}{a_{2,n}} \left\{ \sum_{i=m+1}^{s-1} \left[\left(g_{i+1} - \frac{h_i}{a_{2,n}} \right) e^{-a_{2,n}(t-t_{i+1})} - \left(g_i - \frac{h_i}{a_{2,n}} \right) e^{-a_{2,n}(t-t_i)} \right] \right. \\ \left. - \left(g_s - \frac{h_s}{a_{2,n}} \right) e^{-a_{2,n}(t-t_s)} \right\}, & t_{m+1} < t_s < t \le t_{s+1} \le t_M \\ \\ I_n(t_M) e^{-a_{2,n}(t-t_M)}, & t > t_M \end{cases}$$

Similarly

$$J_p(t) =$$

$$\frac{2qD}{L} \begin{cases} [h_m (t - t_m) + g_m] S_{1,1} \\ -h_m S_{1,2} + \sum_{n=1}^{\infty} \bar{w}_n \alpha_n R_n(t), & 0 \le t_m \le t \le t' < t_{m+1} \\ \\ [h_m (t - t_m) + g_m] S_{2,1} \\ -h_m S_{2,2} + \sum_{n=1}^{\infty} \bar{w}_n \alpha_n R_n(t), & t_m \le t' \le t \le t_{m+1} \\ \\ [h_s (t - t_s) + g_s] S_{2,1} \\ -h_s S_{2,2} + \sum_{n=1}^{\infty} \bar{w}_n \alpha_n R_n(t), & t_{m+1} < t_s \le t \le t_{s+1} < t_M \\ \\ \sum_{n=1}^{\infty} \bar{w}_n R_n(t) \sin(\alpha_n x), & t \ge t_M \end{cases} \tag{A-25}$$

with $R_n(t)$ as above.

Appendix B: Semi-closed form current density FORTRAN computer code

```
!*********************************************************************
!
!  PROGRAM: Jp_piecewise_linear_ss.f90
!
!  PURPOSE: Compute J_p for piecewise linear g(t) using closed-
   form terms
!
!*********************************************************************

      program Jp_piecewise_linear_ss

!     This program will generate a data file of J_p(t) for a
   general piecewise linear
!     g(x,t)
!     This is the version which should be used whenever t_0 <= t^
   prime <= t_M i.e.
!     a neutron pulse occurs during a gamma irradiation.
!     Jp_piecewise_linear_ss.f90 is a modified version of
   Jp_piecewise_linear.f90
!     that uses closed form "steady state" solutions (see sections
    3 and 5 of the SAND report
!     "Analytic 1D pn junction diode photocurrent solutions
   following ionizing radiation and
!     including time-dependent changes in the carrier lifetime
   from a non-concurrent neutron pulse"
!     by Bert Kerr, Carl Axness, and Eric Keiter.


      implicit DOUBLE PRECISION (a-h, o-z)
      DOUBLE PRECISION L , mu, h, I_n, J_p, I_nt_prime,In_endpt,
         J_pss,J_pt
      parameter (nts=50,npts=1000,m=8)
      double precision dt(m)
      real time_begin,time_end
      common/data/ tg(8),g(8),npts_seg(8),In_endpt(10000,8),ifirst
         (10000),I_nt_prime(10000),
     + s11,s12,s21,s22
!     nts = no. of terms in the Fourier Series
!     npts = the number of data points for each segment of the
```

```
   graph,
!     m = number of data points describing g(t)
!     tg(i),g(i) give the time and g the coordinates for the ith
   line segment describing g(t)
!     tg(0)=g(0)=0.
!     t_prime is the time of the neutron strike
!     t_end is the time that the simulation ends
!     All other parameters have names as in the SAND report
!
!  Usage: change parameters, file names, and recomple the program
   for each simulation ...

      open(unit=10, file='Jp_piecewise_E100conv_ss50.dat', status
         ='replace')
      open(unit=11, file='Jp_piecewise_E100conv_ss50.plt', status
         ='replace')
      open(unit=12, file='Jp_piecewise_E100_n50.plt', status='
         replace')

!     Parameters describing the radiation source, indices labeled
   1,2,...
      tg(1)=0.d0
      g(1)=0.d0
      tg(2)=0.5d-6
      g(2)=5.d22      ! 4.3d22 corresponds to 1e9 Rad(Si)/s
      tg(3)=1.d-6
      g(3)=0.d22
      tg(4)=1.5d-6
      g(4)=8.d22
      tg(5)=2.d-6
      g(5)=0.d22
      tg(6)=3.d-6
      g(6)=5.d22
      tg(7)=5.d-6
      g(7)=5.d22
      tg(8)=7.d-6
      g(8)=0.d22          ! m=8 set as a parameter

      write(10,*) 'J_p piecewise data'
      write(10,*)
      write(10,*) (tg(i),i=1,m),(g(i),i=1,m)

!     INPUT THE PHYSICAL PARAMETERS/CONSTANTS these correspond to
   Fig 3, zeta_p=0.5
```

```
      q =  1.602d-19
      D =  11.91d0
      tau1=2.0d-5
      tau2=2.0d-7
      mu = 461.0d0
      E1 = -100.d0
      L = 0.00764d0
      t_prime =  6.0d-6
      t_end = 8.d-6
      pi = 2.d0*dasin(1.0d0)
      a =  mu*E1/(2.0d0*D)
      terma=2.d0*q*D/L
!
! Initial array containing I_n computed at endpoints of segments
!
      call date_and_time
      call cpu_time(time_begin)
!
! compute components of steady-state solution for s1 in terms of
   a1,n
!
      Dtau1=D*tau1
      aL=a*L
      gamma1=dsqrt(a**2+1.d0/Dtau1)
      gamma1L=gamma1*L
      factr=L*tau1/(4.d0*D*gamma1)
      dnum=dsinh(gamma1L)*dcosh(gamma1L)-dexp(-aL)*dsinh(gamma1L)-
     + gamma1L*(1.d0-cosh(gamma1L)*dexp(-aL))
      arg=-a+gamma1*(dcosh(gamma1L)-dexp(-aL))/dsinh(gamma1L)
      s11=L*tau1*arg/2.d0
      s12=L*tau1**2*arg/2.d0-factr*dnum/dsinh(gamma1L)**2
!
! compute components of steady-state solution for s2 in terms of
   a2,n
!
      Dtau2=D*tau2
      gamma2=dsqrt(a**2+1.d0/Dtau2)
      gamma2L=gamma2*L
      factr=L*tau2/(4.d0*D*gamma2)
      dnum=dsinh(gamma2L)*dcosh(gamma2L)-dexp(-aL)*dsinh(gamma2L)-
     + gamma2L*(1.d0-cosh(gamma2L)*dexp(-aL))
      arg=-a+gamma2*(dcosh(gamma2L)-dexp(-aL))/dsinh(gamma2L)
      s21=L*tau2*arg/2.d0
      s22=L*tau2**2*arg/2.d0-factr*dnum/dsinh(gamma2L)**2
      write(10,10) s11,s12,s21,s22
```

```
10    format(//20x,'sij factors for steady state computation',/5x
   ,'s11',9x,'s12',9x,'s21',9x,'s22',
     + /4(e12.4))
      do i=1,nts
        ifirst(i)=0
        do j=1,m
          In_endpt(i,j)=0.d0
        enddo
      enddo

! divide the total number of points to that I_n(t_m) is calculated
    at the end of each line segment
      if(t_end .lt. tg(m)) t_end=tg(m)+tg(m)/npts ! at least 1
         increment at end of simulation
      ntot=0
      do iseg=1,m-1
        npts_seg(iseg)=int((tg(iseg+1)-tg(iseg))*npts/t_end)
        if(npts_seg(iseg) .lt. 1) npts_seg(iseg)=1
        dt(iseg)=(tg(iseg+1)-tg(iseg))/npts_seg(iseg)
        ntot=ntot+npts_seg(iseg)
      enddo
      if(npts .gt. ntot) then
        npts_seg(m)=npts-ntot
        dt(m)=(t_end-tg(m))/npts_seg(m)
      else
        npts_seg(m)=1
        dt(m)=t_end-tg(m)
      endif
! write out number of points in each segment and dt
!       write(10,*) 'g(t) segment information'
!       write(10,*) 'segment no. of pts.        dt          t1
             t2          g1          g2'
!       do iseg=1,m-1
!         write(10,21) iseg,npts_seg(iseg),dt(iseg),tg(iseg),tg(
   iseg+1),g(iseg),g(iseg+1)
!21       format(i5,i14,5(e12.4))
!       enddo
!       write(10,21) iseg,npts_seg(iseg),dt(iseg),tg(iseg),t_end,g(
   iseg)


!     SELECT a sequence of times and compute J_p
!     for t = 0 to t_end

 ! write initial time and current density to the output file, time
```

```
     microseconds
       write(11,41) 0.d0 , 0.d0, 0.d0

      time=0.d0
      do 50 jj=1,m
        do 2 ii=1,npts_seg(jj)

!     COMPUTE the series

          time=time+dt(jj)
          sum = 0.d0
          sign =1.d0
          do n1 = 1,nts
            sign=-sign
            alpha = n1*pi/L
            a1n=D*(alpha**2+a**2+1.d0/(D*tau1))
            a2n=D*(alpha**2+a**2+1.d0/(D*tau2))
            w_nbar=alpha*(1.d0-sign*dexp(-a*L))/(a**2+alpha**2)
            call dI_n(nts,n1,jj,M,time,a1n,a2n,t_prime,t_end,dint,
     +      ss,ii,jj)
            term=w_nbar*alpha*dint
            sum = sum + term
          enddo
          if(time .gt. tg(m)) ss=0.d0          ! steady solution = 0
              here
          J_pss=terma*ss
          J_pt=terma*sum
          J_p=J_pss+J_pt
 ! write the time and current density to the output file, time
    microseconds
          write(11,41) 1.0d6*time , J_pss, J_p
   2    continue
50    continue
! compute the cpu time
      call cpu_time(time_end)
      write(10,*) 'total cpu time for computation with ',nts,'
         terms =',time_end-time_begin

41    format(3(2x,f16.12))
60    format(6(2x,f16.12))
      close(unit=10)
      close(unit=11)
      close(unit=12)
      end program Jp_piecewise_linear_ss
```

```
! Routine to compute the integral I_n(t) see SAND report

      subroutine dI_n(nts,n1,nseg,M,t,a1n,a2n,t_prime,t_end,dint,
         ss,ii,jj)
      implicit DOUBLE PRECISION (a-h, o-z)
      double precision h,I_nt_prime,In_endpt
      common/data/ tg(8),g(8),npts_seg(8),In_endpt(10000,8),ifirst
         (10000),I_nt_prime(10000),
     + s11,s12,s21,s22
! initialize
      sum=0.d0
! If t occurs during pulse then
      if(t .ge. tg(1)) then
 ! if t .le. t_prime, compute I_n
        if(t .lt. t_prime) then
          if(nseg .gt. 1) then
            do j=1,nseg-1
              h=(g(j+1)-g(j))/(tg(j+1)-tg(j))
              term=(g(j+1)-h/a1n)*dexp(-a1n*(t-tg(j+1)))-(g(j)-h/
                 a1n)*dexp(-a1n*(t-tg(j)))
              sum=sum+term
            enddo
          endif
          h=(g(nseg+1)-g(nseg))/(tg(nseg+1)-tg(nseg))
          final_term=-(g(nseg)-h/a1n)*dexp(-a1n*(t-tg(nseg)))
          sum=sum+final_term
          sum=sum/a1n
          ss=(h*(t-tg(nseg))+g(nseg))*s11-h*s12
        else if(t .le. tg(m)) then
! compute I_n for t .ge. t_prime .and. t .le. tg(m)
          if(ifirst(n1) .eq. 0) then
! compute I_n(t_prime) using temporal solution since I_n must
   contain steady state
            ifirst(n1)=1
            sumt_prime=0.d0
            if(nseg .gt. 1) then
              do j=1,nseg-1
                h=(g(j+1)-g(j))/(tg(j+1)-tg(j))
                term=(g(j+1)-h/a1n)*dexp(-a1n*(t_prime-tg(j+1)))-(
                   g(j)-h/a1n)*dexp(-a1n*(t_prime-tg(j)))
                sumt_prime=sumt_prime+term
              enddo
```

```
            endif
! t_prime on first segment
            h=(g(nseg+1)-g(nseg))/(tg(nseg+1)-tg(nseg))
            final_term=h*(t_prime-tg(nseg))+(g(nseg)-h/a1n)*(1.d0-
               dexp(-a1n*(t_prime-tg(nseg))))
            sumt_prime=sumt_prime+final_term
            I_nt_prime(n1)=sumt_prime/a1n
            nsegt_prime=nseg
          endif
! compute I_n for t_prime <= t <= t_{m+1} in SAND report
          if(nseg .eq. nsegt_prime) then
            term1=I_nt_prime(n1)*dexp(-a2n*(t-t_prime))
            h=(g(nseg+1)-g(nseg))/(tg(nseg+1)-tg(nseg))
            final_term=-(h*(t_prime-tg(nseg))+g(nseg)-h/a2n)*dexp
               (-a2n*(t-t_prime))
            sum=term1+final_term/a2n
            ss=(h*(t-tg(nseg))+g(nseg))*s21-h*s22
! If last point on segment, then compute I_n(t_m+1)
            if(ii .eq. npts_seg(jj)) then
              In_endpt(n1,jj)=I_nt_prime(n1)*dexp(-a2n*(tg(nseg+1)
                 -t_prime))+
     +        (h*(tg(nseg)-t_prime)+(h*(t_prime-tg(nseg))-h/a2n)
        *(1.d0-dexp(-a2n*(tg(nseg+1)-t_prime))))/a2n
            endif
          else if (nseg .lt. m) then
! compute I_n for t_{s} <= t <= t_{M} in SAND report
            term1=In_endpt(n1,1)*dexp(-a2n*(t-tg(nseg)))
            if(nsegt_prime .lt. nseg-1) then
              do j=nsegt_prime+1,nseg-1
                h=(g(j+1)-g(j))/(tg(j+1)-tg(j))
                term=(g(j+1)-h/a2n)*dexp(-a2n*(t-tg(j+1)))-(g(j)-h
                   /a2n)*dexp(-a2n*(t-tg(j)))
                sum=sum+term
              enddo
            endif
            h=(g(nseg+1)-g(nseg))/(tg(nseg+1)-tg(nseg))
            final_term=-(g(nseg)-h/a2n)*dexp(-a2n*(t-tg(nseg)))
            sum=sum+final_term
            sum=term1+sum/a2n
            ss=(h*(t-tg(nseg))+g(nseg))*s21-h*s22
            if(ii .eq. npts_seg(jj)) then
              In_endpt(n1,jj) = In_endpt(n1,jj-1)*dexp(-a2n*(tg(jj
                 )-tg(jj-1)))+(h*(tg(nseg+1)-tg(nseg))+
     +        (g(nseg)-h/a2n)*(1.d0-dexp(-a2n*(tg(nseg+1)-tg(nseg)
        )))))/a2n
```

```
            endif
          endif
        else
!    t occurs after pulse, compute sum using I_n(t_M)
          sum=In_endpt(n1,nseg-1)*dexp(-a2n*(t-tg(m)))
        endif
      else
! case where t<tg(1), assumed that there is no pulse so dint=0
        write(10,*) 't < t(1), no irradiation assumed during this
           period'
        sum=0.d0
      endif
      dint=sum
      end
```

DISTRIBUTION:

1	MS 1179	Harold Hjalmarson, 01341
1	MS 1179	Leonard Lorence, 01341
1	MS 0824	Joel Lash, 01510
1	MS 1167	Michael McLain, 01343
1	MS 0352	Chuck Hembree, 01344
1	MS 1159	Kyle Mcdonald, 01344
1	MS 1146	Donald King, 01384
1	MS 1146	Patrick Griffin, 01384
1	MS 0316	Rob Hoekstra, 01426
1	MS 0316	Eric Keiter, 01445
1	MS 0316	Richard Schiek, 01445
1	MS 0316	Heidi Thornquist, 01445
1	MS 0316	Joe Castro, 01445
1	MS 0316	Tom Russo, 01445
1	MS 1083	Paul Dodd, 01731-1
1	MS 1072	Nathan Nowlin, 01731
1	MS 0779	Carl Axness, 06784
1	MS 9007	Dean Clark, 8245
1	MS 9154	Brian Owens, 8244
1	MS 1056	Bill Wampler, 01111
1	MS 1415	Sam Myers, 01110
1	MS 0899	Technical Library (electronic copy), 09536
1	Dr. Bert Kerr Mathematics Dept. NM Tech Socorro, NM 87801	

Sandia National Laboratories